Application of Highly Modified Asphalt (HiMA) Binders in Implementation and Thickness Optimization of Perpetual Pavements in Ohio

A thesis presented to

the faculty of

the Russ College of Engineering and Technology of Ohio University

In partial fulfillment

of the requirements for the degree

Master of Science

Paul F. Cichocki

August 2015

This thesis titled

Application of Highly Modified Asphalt (HiMA) Binders in Implementation and Thickness Optimization of Perpetual Pavements in Ohio

by

PAUL F. CICHOCKI

has been approved for

the Department of Civil Engineering

and the Russ College of Engineering and Technology by

Shad M. Sargand

Russ Professor of Civil Engineering

Dennis Irwin

Dean, Russ College of Engineering and Technology

ABSTRACT

CICHOCKI, PAUL F., M.S., July 2015, Civil Engineering

Application of Highly Modified Asphalt (HiMA) Binders in Implementation and Thickness Optimization of Perpetual Pavements in Ohio

Director of Thesis: Shad M. Sargand

This research explores using highly modified asphalt (HiMA) mixtures as an alternative to standard materials in furtherance of making perpetual pavements thinner in Ohio. Previous projects on I-77, US Route 30, and US Route 23 have demonstrated that reduced strains were possible with standard materials at greater pavement thicknesses. Thinner and superior pavements with improved binder have the potential to reduce the construction cost of perpetual pavements, despite the higher unit cost of materials.

Four test sections containing HiMA with varying base layer thicknesses of 8 in, 9 in, 10 in, and 11 in were installed at the Accelerated Pavement Loading Facility (APLF) in Lancaster, Ohio. To successfully compare the effect of the HiMA in the various thicknesses, the 11 inch section acted as a control with a non-modified base layer. Each pavement was subjected to 10,000 passes of a single axle load of 9000 lbs at two pavement temperatures of 70°F and 100°F. Rutting on the surface of the pavement was measured using a rolling wheel profiler after 100, 300, 1000, 3000, and 10,000 wheel passes, while pavement distresses were found at the bottom of the base and intermediate layers in the longitudinal and transverse directions after wheel passes of 100, 3000, and 10,000 at wheel loads of 6000, 9000, and 12,000 lbs. The serviceability of the pavements was determined by comparing the longitudinal tensile strains within the base layer of

each pavement to calculated fatigue endurance limits (FEL) found by using flexural stiffness standards from NCHRP Design Guides in addition to Kansas researchers to determine which sections met the perpetual design concept.

Following the testing, it was determined that the four test sections showed no significant rutting damages after being subjected to 20,000 passes of a single axle load of 9000 lbs. Additionally, the thinnest section produced maximum average strains higher than the calculated fatigue endurance threshold at 100°F using the NCHRP 9-44A equation; however, using the Kansas researchers approach, all four test sections were found to have lower longitudinal strains than the calculated FEL. The findings from this study have shown that the modified binder provides substantial improvement in rutting but did not show significant improvements in structural support when comparing the modified asphalt to standard asphalt mixtures.

DEDICATION

To my family and friends for their support and encouragement through my schooling journey, without you this wouldn't have been possible

ACKNOWLEDGMENTS

First and foremost, I would like to thank the civil engineering facility and staff at Ohio University for all of their guidance and exemplary teachings they have given to me throughout the time I have attended this university. The education I have gained from you all will serve as my foundation as I continue the next chapters in my life. Amongst the facility and staff, I need to especially thank Issam Khoury. Throughout my 6 years spent here at Ohio University Issam has always been extremely encouraging and if not for his persistence towards the graduate program I may have never decided to pursue this achievement. I would also like to thank him for all of the support and expertise given to me during the installation phase of my project. In addition, I would like to thank Ben Jordan for all of his guidance throughout my project and for his continuous help throughout the graduate program. Without his insights from past projects my understanding of perpetual pavements would be substantially narrowed. Furthermore, I would like to thank Roger Green for spending countless hours in the APLF running the load machine and for all of his knowledge bestowed to me. Finally, I would like to thank my advisor, Dr. Sargand. Over the past two years, I have been able to learn from an individual who has contributed such a great deal towards the civil engineering community. I especially want to thank Dr. Sargand for giving me the opportunity to pursue this achievement.

TABLE OF CONTENTS

Page

LIST OF TABLES

Page

LIST OF FIGURES

CHAPTER 1: INTRODUCTION

1.1 Problem Statement

Common roadway design goals are for pavements to be environmentally friendly, durable, and economical; however, it is not always possible to optimize all three goals and engineers are often left with a give and take scenario. With the growing population and increasing volume of vehicles on the roadways, these goals have become more difficult to maintain. According to the Federal Highway Administration (FHWA, 2013), in 2010 a total of 33.8 billion dollars was spent between the federal, state, and local branches of government on highway maintenance in the United States. Perpetual asphalt pavements have the sustainability needed and the longer service lives to impact pavement designs (Newcomb et al., 2010). With the United States having more than 90% of the roadways using asphalt surfaces (Asphalt Pavement Alliance, 2010), the need for a more durable asphalt pavement that can cope with high volumes of traffic while still maintaining an economical cost is desired.

Typical distresses found in asphalt pavements are rutting and bottom up fatigue cracking, which are both caused by a weak or poor asphalt binder among many other causes (Roberts et al., 2002). Improving the asphalt binder would allow for higher levels of fatigue resistance in the pavement; therefore, an overall improvement in bottom up fatigue cracking can be seen even at higher levels of tensile strain than usual near the base of the pavement. Furthermore, an improved asphalt binder may be used to stiffen the surface layer of an asphalt pavement, thus leading to a pavement that would be more resistant to rutting.

Fatigue cracking and rutting can cause complete failure in roadways and many individuals would agree that without functioning roadway systems, their daily lives would be negatively impacted. In the past, full depth and deep strength hot mix asphalts (HMA) pavements were designed to have a service life of about 20 years, but according to Newcomb et al. (2001), with the addition of new materials, a more durable and thinner perpetual pavement can be created. This perpetual pavement would be designed to have a service life of 50 years or more with rehabilitation occurring every 20 years to the surface layer. Since the pavements are thinner and have an increased service life, money can be saved in materials and construction costs. Using this concept of perpetual pavement with the addition of a high polymer asphalt binder, a highly modified asphalt pavement (HiMA) can be created. This HiMA creates an impermeable and durable surface layer that stops rutting from occurring, while creating an intermediate layer that withstands higher tensile strains in the bottom of the base layer to prevent bottom up fatigue cracking. With this HiMA pavement, the service life may become higher and the overall depth of the asphalt is decreased.

In order to further develop the optimal design for perpetual pavements in Ohio, a joint venture was created between Ohio Department of Transportation (ODOT), Ohio Research Institute of Transportation and the Environment (ORITE), and Flexible Pavements of Ohio. A total of 4 highly modified asphalt (HiMA) pavements with changing base thicknesses of 8 in (20 cm), 9 in (22.5 cm), 10 in (25 cm), and 11 in (27.5 cm) were constructed on a 6 in (15 cm) dense graded aggregate base with chemically stabilized subgrades. The HiMA pavements were tested in the Accelerated Pavement

Loading Facility (APLF) and representative samples were compacted. Those compacted samples volumetrics were measured and dynamic modulus were determined.

In this thesis, the strains were measured in the bottom of the intermediate and base layer in both the longitudinal and transverse directions to determine maximum strains throughout the HiMA pavements. Temperature sensors were embedded into the HiMA pavement while air temperatures were controlled to simulate realistic field conditions. Moreover, the results gained from the laboratory tests provided the engineering properties of the HiMA pavement, which were used with the Mechanistic-Empirical pavement design method to provide an optimum pavement structure.

1.2 Objectives

The principal objectives of this study are as followed:

- Investigate 4 perpetual pavement structures containing highly modified asphalt (HiMA) with varying AC Base thicknesses.
- Study the effect of an increase in temperature on the rutting and strains within each HiMA pavement.
- Study the effect of wheel position over pavements with respect to strains in each layer of the pavements.
- Analyze longitudinal and transverse strains in each of the pavements corresponding to where each gage is located.
- Determine the optimal design thickness of HiMA structure for perpetual pavements in Ohio.

1.3 Outline

Chapter 1 introduces and defines the history of perpetual pavement as well as states the objectives of the research.

Chapter 2 is a literature review on perpetual pavements. It describes different perpetual pavement designs, failure modes, polymer additives, and past perpetual structure locations.

Chapter 3 provides a background on the preparation and implementation of the HiMA pavement, and presents the installation of the gauges used in the APLF.

Chapter 4 discusses and interprets the results collected during dynamic testing conducted in the APLF and laboratory testing.

Chapter 5 states general overall conclusions found from this study and includes recommendations for future works in this field.

CHAPTER 2: LITERATURE REVIEW

Asphalt pavement in the United States account for more than 90% of the total roadway systems (Asphalt Pavement Alliance, 2010). With such a large portion of the country using asphalt pavements, it is imperative that the roadways be designed to their optimal levels. Over the years, the design processes for asphalt pavements have been continually changing. Currently, the mechanistic empirical pavement design (M-E) is being used for perpetual pavements. The M-E design uses a wide range of pavement parameters as inputs with an iterative process to predict how well the pavement structure will perform in terms of pavement distresses. In order for the design to be accepted, the M-E design must meet the design criteria of each given site. Although the M-E design is effective, the changing of the materials and new additives being used in asphalt binders may mean that a new asphalt design approach may be necessary. Within this chapter, perpetual pavement will be defined, different perpetual pavement designs discussed, current experimental asphalt sites examined, and highly modified asphalt explained.

2.1 Perpetual Pavement

Since the typical design life of conventional asphalt pavements is 20 years, the majority of pavements in use today have been designed using the 1993 American Association of State Highway and Transportation Officials (AASHTO) Guide for Design of Pavement Structures. The guide primarily used data found from tests conducted at the 1950's AASHTO Road Test where pavements were subjected to 8 million equivalent single axle loads (ESALS), known vehicle loads, and known pavement thicknesses while damages to the pavements were monitored. From these results, AASHTO developed a design guide for flexible and rigid pavements; however, flexible pavements in use today have been designed for much larger ESALS and are ultimately forcing engineers to extrapolate from the design guide (Newcomb et al., 2010). This extrapolation has caused many of the asphalt pavements to become vastly over-designed.

A pavement section thickness in the past was reduced through the use of thicker HMA layers to replace granular base courses (Newcomb & Hansen, 2006). The over-designing problems that occurred when designing for longer service lives in asphalt pavements led to the concept of perpetual pavement (Newcomb et al., 2010). The first concept of perpetual pavement was developed in 2002 by the Asphalt Pavement Alliance (APA). According to the APA (2002), a perpetual asphalt pavement has an extended service life of beyond 50 years and requires negligible structural rehabilitation or reconstruction. Although the pavement cannot have major structural repairs to the base and intermediate layers, the APA allows for repairs to be made on the surface layers every 15 to 20 years (APA, 2010).

To improve on the 1993 AASHTO design guide the mechanistic empirical pavement design was developed. Using a variety of pavement parameters such as climate, traffic, and mixture properties, pavements could be more accurately designed. Incorporating the same design parameters used within the M-E pavement design with an addition of a fatigue endurance limit (FEL), Thompson and Carpenter (2006) suggested that this design approach could be used to more accurately design asphalt pavements to meet the APA requirements for perpetual pavements. Furthermore, in addition to the perpetual pavement qualifications created by the APA, two additional qualifications were suggested by Thompson and Carpenter (2006). They proposed that the pavements in question must keep flexural strains below the FEL during the hottest month of the year. Yet, if the pavement fails to reach that circumstance, a second condition that states for some other hot months the flexural strain in the pavement must fall below the FEL (Thompson and Carpenter, 2006).

Past research has shown that perpetual pavements provide a superior life cycle cost analysis than traditional asphalt pavements (El-Hakim et al., 2009). The extended service lives of perpetual pavements with minor repairs being limited to the surface layer provides beneficial opportunities to the state DOT's. Timm and Newcomb (2006) stated that these pavements can offer shorter pavement rehabilitation times and an overall lower life cycle cost compared to traditional asphalt pavements. The rapid repair ability associated with asphalt pavements allow for pavement repairs to be accomplished at times that cause minimal user delays (APA, 2010). Areas such as highways that see high volume of traffic or urban roadways economically benefit the most by using perpetual pavements (Tarefder & Bateman, 2009). Reducing factors such as life cycle costs, user delays, and operational costs allow for an overall increase in productivity within the United States infrastructure.

Further studies and advances in pavement technologies have allowed for perpetual pavements to become a more realistic goal rather than just an intangible concept. According to Newcomb & Hansen (2006), some perpetual pavements have existed as early as the 1960's from the overdesigned HMA layers. These pavements by today's standards could be considered to meet the perpetual pavement qualifications. Research conducted by Jordan (2014) found seven pre-existing sites across Ohio that exhibited perpetual qualifications. Between 2001 and 2013, the Asphalt Pavement Alliance has selected 93 asphalt pavements, within the United States, to receive the Perpetual Pavement Award. To qualify, at least 35 years of service is needed for each pavement and the pavements cannot exceed an overlay increase of four inches (Newcomb et al., 2010).

Although perpetual pavements are designed to far surpass traditional asphalt pavements through performance, pavement distresses occurring from external stresses will continue to be the driving force in pavement design.

2.2 **Pavement Distresses**

In order for any pavement to perform to its optimal capabilities the structure must be able to maintain its design without any flaws. These flaws in pavements can occur at any scale and any location within the pavement itself. Typically, many of these flaws cannot be determined until the pavement has already become structurally damaged. These damages are often caused by strains, stresses, and displacements that take place over the pavements service life. If these pavement rehabilitations go without repair or are not completed periodically, even previous APA perpetual pavement award winning pavements can perform poorly, as shown by Heitzman and Coree (2004) report of I-80. The idea in perpetual pavement design is that asphalt pavements are designed to keep these damages below the threshold in which structural damage will occur (Newcomb et al., 2010). Considering perpetual pavement designs today, the two most common pavement distresses examined are rutting and bottom up fatigue cracking.

2.2.1 Rutting

When the asphalt pavement structure is unable to support an applied wheel load, the material within the pavement is displaced (Adlinge & Gupta, 2013). This permanent deformation known as rutting, takes place at wheel paths on an asphalt pavement. This displacement of materials within the asphalt creates a channel and depending on the severity of the rut, the channels can hold still water causing major traffic hazards for any automobile driver.

Since the asphalt pavement is constructed in various layers, there is a potential for rutting to occur in multiple layers. Surface rutting typically occurs within the first few inches of the asphalt pavement, whereas structural rutting takes place in the base layer and into the subgrade (Newcomb et al., 2010). Depending on the type of rutting, there are different approaches that can be used to repair asphalt pavements. According to Adlinge and Gupta (2013), there are three possible outcomes when dealing with rutting in asphalt pavements. For shallow rutting within the surface layer, micropaving can be used as a treatment. The second outcome, deeper ruts are to be filled to meet the existing pavement height followed by a stiffer overlay. Finally, if there is a poor subgrade or structural cracking occurs, reclamation or reconstruction may be the outcome.

2.2.2 Fatigue Cracking

Most pavements are designed to be traveled on repeatedly by cars and other transportation devices, however; these repeated traffic loads can often prove to be detrimental to pavement structures. Repeated loads cause cracks to form in the surface or base of the asphalt pavement (Adlinge and Gupta, 2013). According to Moreno and

Rubio (2013), in addition to stresses caused by the repeated loadings, fluctuating temperature within the pavement causes additional strains to occur. These additional temperature strains with the repeated loadings cause the pavement structures to begin to crack and ultimately lead to failure within the pavement.

2.3 Fatigue Endurance Limit (FEL)

With asphalt pavement being constructed in various layers, having a crack propagate to the surface layer from the base is the fatigue failure. Fatigue cracking, better known as bottom-up cracking, starts when strains in the base of a pavement surpasses the structures maximum allowable strain threshold. This strain threshold is referred by engineers as the fatigue limit. Since different binders, depth, and materials are used in asphalt pavements to accommodate specific requirements, the fatigue limit is unique to each asphalt pavement. According to Nunn et al. (1997), it was discovered in varying thickness asphalts that at certain points the thicknesses in asphalt pavements eventually reached a strain limit where distresses such as fatigue cracking and structural rutting ceased to occur. Many engineers believe that there is a universal fatigue endurance limit that exists, and that keeping tensile strains in the flexible pavement base below this limit will significantly improve the pavements service life (Monismith and McLean, 1972; Newcomb et al., 2010; Witczak et al., 2013).

As mentioned before, most engineers have agreed that a limit does exist; however, the exact endurance limit has been a topic of discussion. This fatigue endurance limit was first suggested by Monismith and McLean (1972) to be 70 mircostrains for HMA pavements. Since this time, testing has continued on the fatigue endurance limit providing varying results. Carpenter et al. (2003) validated the work completed by Monismith and Mclean and further hypothesized that the fatigue endurance limit could fall into a range between 70 to 90 microstrains; however, in 2010 the National Cooperative Highway Research Program (NCHRP) conducted further investigation on the FEL in their Report 646. In this report Prowell and colleagues (2010), agreed that the FEL limit existed in HMA pavements but varied between 75 to 200 microstrains depending on specific mixture properties of the HMA.

In more recent studies, it has been hypothesized that the endurance limit not only changes due to mixture properties in HMA pavements but must also change throughout the year due to the healing that occurs within the asphalt binders (Witczak et al., 2013). In the NCHRP project 9-44A, they concluded that the endurance limit could fall between 22 to 264 microstrain, and that during high temperatures the endurance limit proved to be larger than low temperatures. In an attempt to relate various mixture properties, rest periods, and number of loading cycles that affect the FEL, Witczak et al. (2013) developed the following model from beam fatigue tests:

$$\begin{aligned} \boldsymbol{SR} = \quad & \mathbf{2.0844 - 0.1286 * \log(\boldsymbol{E_0}) - 0.4846 * \log(\boldsymbol{\varepsilon_t}) - 0.2012 * \log(\boldsymbol{N})} \\ & \mathbf{+ 1.4103 * \tanh(0.8471 * \boldsymbol{RP}) + 0.0320 * \log(\boldsymbol{E_0}) * \log(\boldsymbol{\varepsilon_t})} \\ & \mathbf{- 0.0954 * \log(\boldsymbol{E_0}) * \tanh(0.7154 * \boldsymbol{RP}) - 0.4746 * \log(\boldsymbol{\varepsilon_t})} \\ & \mathbf{* \tanh(0.6574 * \boldsymbol{RP}) + 0.0041 * \log(\boldsymbol{N}) * \log(\boldsymbol{E_0}) + 0.0557} \\ & \mathbf{* \log(\boldsymbol{N}) * \log(\boldsymbol{\varepsilon_t}) + 0.0689 * \log(\boldsymbol{N}) * \tanh(0.2590 * \boldsymbol{RP})} \end{aligned}$$

Eq. 1

Where:

SR = Stiffness Ratio

E_0 = Initial Flexural Stiffness (ksi)

ε_t = Applied Tenisle Strain (με)

$RP = \text{Rest Period (seconds)}$

$N = \text{Number of Load Cycles}$

According to Witczak et al. (2013), inputting a value of 1.0 as the stiffness ratio and back-calculating the tensile strain would produce the FEL for a specific asphalt mix.

2.4 Asphalt Pavement Design

Providing a smooth ride, strong traction, subgrade support, and a watertight pavement are the primary purposes of an asphalt pavement (Adlinge & Gupta, 2013). Manipulation of the structural design as well as the physical composition can be modified to provide asphalt pavements with the characteristics mentioned by Adlinge & Gupta. Asphalt pavements are designed using a multi-layered system that is used to dissipate stresses from the uppermost layer through to the subgrade. The most typical asphalt pavement design consists of a surface layer, intermediate layer, and a base layer (Tarefder and Bateman, 2009). Each layer has a distinctive purpose in the designing of an asphalt pavement and will be discussed in greater detail below.

2.4.1 Surface Course

The uppermost section of the pavement layers is known as the wearing course or surface course layer. According to Newcomb & Hansen (2006), the surface layer experiences the largest fluctuation of temperature as well as the highest vertical stresses of any of the pavement layers. These high levels of vertical stresses are caused by a combination of two major factors, the lack of separation between the wheels and the interface of the pavement as well as the thermal stresses caused by the temperature changes. In addition to withstanding the high stresses caused by these conditions, Adlinge & Gupta (2013) state the surface layer must satisfy other characteristics such as providing a smooth ride, having high surface friction, and preventing the seepage of water in subsequent pavement layers. The addition of standing water on pavement structures often leads to many hazardous conditions for drivers. Tarefder and Bateman (2009), suggest that materials such as Stone Matrix Asphalt (SMA) or Open Graded Friction Course (OGFC) can help remediate issues caused by standing water. To compensate for all these characteristics the surface course mix design typically uses the highest quality of materials of any of the subsequent pavement layers (Garcia & Hansen, 2001).

With the highest levels of stresses occurring in this layer, major pavement distresses such as rutting and cracking are typically associated within the surface course layer. According to Yildirim (2007), polymer modified asphalt binders have shown substantial improvements over traditional asphalt binders in terms of rutting, thermal cracking, and fatigue cracking. In addition, Newcomb and Hansen (2006) suggested with the addition of polymers in asphalt mixes thermal cracking in pavements could be significantly reduced while pavements experienced lower temperatures.

2.4.2 Intermediate Course

The intermediate course layer, or binder course layer, acts as a buffer between the surface course layer and the asphalt concrete base layer in a typical pavement layer design system. Intermediate layers must provide adequate rut resistance as well as be durable enough to withstand high levels of stresses produced by traffic loadings (Tarefder and Bateman, 2009). According to Garcia & Hansen (2001), the intermediate layer is primarily used to further dissipate the high level of stresses caused by traffic loading such that no permanent damages are created in the succeeding base layer. They also reported that the intermediate layer design has a significant impact on the mix design and thickness of the surface layer (Garcia & Hansen, 2001).

Since the location of the intermediate layer falls between the surface and base course layers, the intermediate layer must have similar characteristics to both. Characteristics such as smoothness of the surface layer and the ability to decrease stresses faster than the surface course can be aided by the use of larger size aggregate in the intermediate layer (Newcomb & Hansen, 2006). They further hypothesized that if high traffic volumes are expected, the combined use of crushed aggregate and polymer modified asphalt could be used to reduce the rutting throughout the asphalt pavement (Newcomb & Hansen, 2006).

2.4.3 Asphalt Concrete Base Course

The asphalt concrete (AC) base, the lowest asphalt layer in traditional flexible pavement structures, can be located either on an aggregate base course or directly on the subgrade if an aggregate base was deemed unnecessary. The AC base layer, unlike the surface and intermediate course layers, experiences the highest levels of tensile strains within the asphalt pavement primarily caused by repeated traffic loadings and are focused at the bottom of the AC base layer. These high levels of strains caused from repeated traffic loadings are often associated with fatigue cracking (Adlinge & Gupta, 2013). In order to better resist permanent deformation caused by the high levels of tensile strains, the AC base layer must be more durable and fatigue resistant than the previous layers (Newcomb and Hansen, 2006).

Field and laboratory studies in flexible pavement designs have discovered that the high levels of tensile strains that causes fatigue cracking found in the AC base can often be remediated through a few different methods. According to El-Hakim et al. (2009), fatigue cracking can be eliminated in AC base layer by providing an adequate amount of total pavement thickness such that tensile stress in the base layer never surpasses the tensile strength of the AC base. However, Newcomb et al. (2010) suggest that although this method works, often pavements are increased well beyond the needed resistant strain levels and often lead to higher financial as well as economical costs. A report by Tarefder and Bateman (2012) suggested that rather than increasing the thickness of a pavement the use of a higher binder content to increase the flexibility by decreasing the permeability of the AC base layer could be utilized.

Not until more recently has the concept of using modified binders in the AC base layer become an area of flexible pavement studies. With the AC base layers of flexible pavements experiencing lower temperature gradients than the surface and intermediate layers, the addition of modified binder use in the AC base was rarely tested (Willis et al., 2012). According to Kluttz et al. (2009), the fatigue resisting capabilities of highly modified binders being used in the AC base layer could further reduce layer thicknesses within asphalt pavements.

2.4.4 Aggregate Base Course

The aggregate base, or subbase, is an optional layer that is on top of the subgrade and is comprised of crushed granular aggregate. The durable aggregates in the subbase help the above asphalt layers in further protecting the subgrade in frost susceptibility and water drainage. According to Newcomb et al. (2010), the thickness of an aggregate base is dependent on the California Bearing Ratio (CBR) of the subgrade. Furthermore, subgrades with a CBR lower than 6 should make use of a dense graded aggregate base (DGAB) for additional subgrade support (Newcomb et al., 2010). Since stresses in the aggregate base are dispersed more over an area compared to the surface course, weaker materials are often used in lower layers to increase flexibility (Adlinge and Gupta, 2013).

2.4.5 Subgrade

The foundation, or bottom of a pavement, is known as the pavements subgrade. The main objective of this pavement section is to support the various preceding layers of the asphalt pavements. Subgrade factors affecting asphalt pavement designs include frost susceptibility, bearing capacity, and shrink-swell (El-Hakim et al., 2009). Von Quintus (2001) suggested that subgrades should have a minimum resilient modulus of 25 ksi to ensure the support of the preceding asphalt layers. Weak or poorly constructed subgrades can cause pavements to fail. The introduction of moisture in subgrade, either through seepage through the pavement or moisture from surrounding areas around the pavement, drastically changes the strength properties of the subgrade (Adlinge & Gupta, 2013). However, as mentioned earlier in this chapter, compositional changes in the above asphalt layers can be changed to prevent seepage of moisture from reaching the subgrade.

Recent advances in subgrade research have discovered that mechanical and chemical soil stabilizations can be used in strengthening subgrades (Sargand et al., 2014, Tarefder and Bateman, 2009, El-Hakim et al., 2009). Two common chemical stabilizations currently being used to strengthen subgrades are lime and cement treatments. Of the two, lime stabilization reacted the most with soils with medium to fine graded particles allowing for better resistance of swelling and a reduction of plasticity in the soils; whereas, cement stabilization reacted best with well graded aggregates allowing for stronger soils (Little and Nair, 2009). Improving the resilient modulus in the subgrade can result in better rutting protection of the above asphalt layers (Tarefder, 2012). The study by Sargand et al. (2014) showed that using chemically stabilized subgrades resulted in higher resilient modulus in the subgrade. In addition, their results showed that the increased subgrade modulus allowed for the aggregate base modulus to increase as well due to better compaction caused by the strengthened subgrade (Sargand et al., 2014).

2.6 Perpetual Pavement Site Investigations

To continuously advance further in pavement technologies forensic site investigations have been conducted across the United States. The following pavement locations discussed below shed further background on studied perpetual pavements.

2.6.1 Accelerated Pavement Load Facility (APLF)

A wide range of pavement studies have been conducted in the APLF since it was constructed in 1997; however, only one perpetual asphalt pavement study prior to this current research had been completed in the APLF.

Research was conducted by Sargand et al. (2009) on asphalt pavements to analyze the advantages of using warm mix asphalts (WMA) compared to traditional hot mix asphalts. The research compared three different WMA surface mixtures that contained a different additive (Evotherm, Aspha-Min Zeolite, or Sasobit) to a conventional HMA. Within the APLF, a total of eight sections containing the four different surface mixtures were constructed on two sets of perpetual pavement thicknesses, as seen in Figure 2.1.

According to Sargand et al. (2009), testing was performed in each section to measure dynamic responses as well as surface rutting at three temperatures (40°F (4.4°C), 70°F (21.1°C), and 100°F (37.8°C). The dynamic responses were measured using a falling weight deflectometer (FWD) as well as a dynamic dual tire wheel. Each method used loads of 6000 lb (27 kN), 9000 lb (40 kN) and 12,000 lb (53 kN). Profiles were taken to measure rutting of each test section prior to loading and upon completion of 100, 300, 1000, 3000, and 10,000 passes of a 9000 lb (40 kN) load.

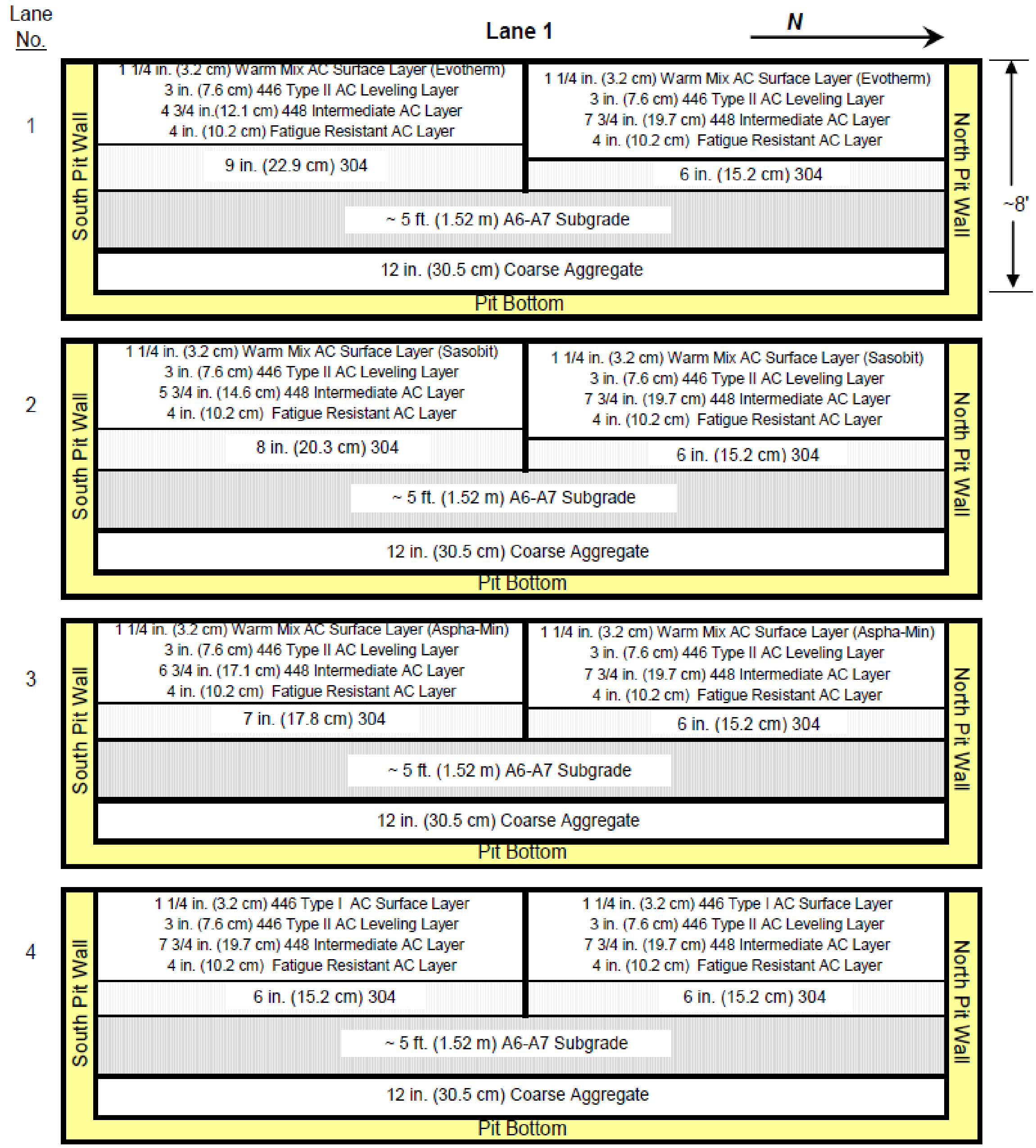

Figure 2.1 Test Sections Profile in APLF from WMA Study (adapted from Sargand et al., 2009)

Sargand et al. (2009) concluded from the WMA APLF study that there were no significant differences in strains found at the base of the Fatigue Resistant Layers;

therefore, a pavement reduction from 16 in (41 cm) to 13 in (33 cm) with an increase in AC base would be acceptable. Rutting findings showed that the three WMA sections underperformed the HMA control section during early wheel passes but as testing continued both the WMA and HMA sections experienced equal rutting (Sargand et al., 2009).

2.5.2 State Route 23 in Delaware, Ohio

Further advances in perpetual pavement studies were conducted by Scheer (2013) on State Route 23 in Delaware, Ohio. A total of four multiple layered sections with varying thicknesses of 15 in, 13 in, 13 in, and 11 in. asphalt pavements were analyzed in an attempt to minimize the depth of asphalt pavements in Ohio. Each test section was built on top of a 6 in dense graded aggregate base (DGAB) and contained a 4 in fatigue resistant layer that was built above the asphalt base layer. The 11 in and 13 in asphalt sections were constructed with a lime stabilized subgrade, while the other 13 in and 15 in sections contained no chemical subgrade stabilization.

Strains and temperature for each test section were recorded throughout the full depth of the asphalt pavement structures during the winter of 2012. Due to complications during construction, data from the 13 inch asphalt section with no chemical stabilization was not recorded for the report. Scheer (2013) stated from in field testing that the 13 inch section with stabilized subgrade yielded pavement strain responses lower than the 15 inch section without any chemical stabilization. PerRoad analysis conducted by Scheer (2013) projected each of the tested sections to have a lifespan far beyond 50 years with pavement responses falling below their maximum threshold 99% of the time.

2.5.3 National Center for Asphalt Technology (NCAT) Test Track

Significant developments in asphalt pavements have been discovered from tests conducted at the NCAT pavement test track in Opelika, Alabama. According to Willis et al. (2009), the track was designed to be a closed-circuit that contained 46 test pavements and each section would be subjected to 10 million ESALs over a span of two years. Throughout testing, the test pavements were monitored at various locations, measuring pavement characteristics such as: strains, vertical pressure, rutting, cracking, and temperatures.

According to Timm et al. (2013), a 5.75 in highly polymer modified asphalt (HPM) was designed with 7.5% styrene-butadiene-styrene polymer and compared to a 7 in asphalt section containing conventional materials on the NCAT test track. Each of the two asphalt concrete sections was constructed having similar aggregate gradations and built over a 6 in granular base. Data was recorded over a span of two years with each section being subjected to over 10 million ESALs. Findings from this study concluded that neither section showed any sign of cracking, but laboratory tests showed a significant improvement in rutting resistance in the HPM asphalt over the conventional asphalt as well as showed an estimated increase of fatigue life by 17 times that of the conventional asphalt (Timm et al., 2013)

2.6 Highly Modified Asphalt (HiMA)

Enhancing specific properties within asphalt pavements have shown to be beneficial in pavement performances. Typical polymer asphalt modifications contain 2% to 3% in terms of asphalt volume and can swell 5 to 10 times the original volume (Timm et al., 2011). According to Yildirim (2007), polymer modifications completed to asphalt binders have shown an increase resistance in rutting and fatigue damages. Similar to using different types of aggregates in mix designs to meet layer specific requirements; different types of polymers are utilized in much of the same way. The addition of different polymers in asphalt binders have been found to increase elastic recovery while providing higher levels of ductility in asphalt pavements (Yildirim, 2007). Although different polymer additives are employed, currently over 60% of the polymer modified asphalt pavements globally use Styrene-Butadiene-Styrene (SBS) on account of the SBS polymers increased ability to resist rutting and cracking (Molenaar et al., 2011).

Early uses of polymer modified asphalts had originally been limited to the surface layers of asphalt pavements because of the high levels of stresses and temperature changes associated with this layer; however, Kluttz et al. (2009) suggested that utilizing polymer modification within the intermediate and base layers can provide an overall reduction of the pavement depth compared to traditional hot mixed asphalt pavements. A report by Timm et al. (2011) suggested that an increase in polymer percentage to 7% by volume weight would provide a higher fatigue and rut resistance modified asphalt than the traditional polymer modified asphalt; however, they suggested that additional paving challenges would arise.

CHAPTER 3: METHODOLOGY

3.1 APLF Project site

In cooperation with ODOT, the APLF study continued research on optimizing perpetual pavements in the state of Ohio. To further this research, a new modified binder created by Kraton Polymers that contains a 7.5% styrene butadiene styrene (SBS) polymer was used at the APLF in Lancaster, Ohio. Currently, this HiMA mixture is being investigated at the National Center for Asphalt Technology (NCAT) test track near Auburn, Alabama. Based on the findings thus far at the NCAT test track, four test sections with the highly modified asphalt were set up in the APLF. The four test sections varied in thicknesses between 8 in (20 cm) and 11 in (28 cm) in order to determine where the pavement transitions from standard to perpetual performance.

The Accelerated Pavement Loading Facility consists of a 45 feet (13.7 m) length by 38 feet (11.6 m) width by 8 feet (2.5 m) depth rectangular pit that is bounded by concrete walls. The facility has two large sliding doors on the north and south ends of the facility, which allows large construction vehicles to enter and exit freely, a feature which makes the APLF unique. As an indoor facility, tests may be performed at any time of the year. The facility also houses industrial grade heating and cooling units to test and maintain pavements at desired temperatures, which can be anywhere from 10°F (-12.2°C) to 130°F (54.4°C). Dynamic and static wheel testing can be accomplished by either a dual or single wide-based tires. The wheel is mounted onto a track system that is supported by two I-beams. The mounted wheel support feature allows for the ability to maintain a desired wheel load and pressure at a precise location for repeated loadings on a test pavement. The APLF is capable of a wheel load of up to 30,000 lbs (133 kN) with the option of wheel offsetting to measure wander effects. A dynamic loading test from inside the APLF can be seen in the following figure.

Figure 3.1: APLF Running Test

3.2 Instrumentation of APLF

In an agreement with the Ohio Department of Transportation (ODOT), it was decided to use an instrumentation plan similar to those employed in prior perpetual pavement studies (Sargand et al., 2009); therefore, strain gages, thermocouples, and linear variable differential transformers (LVDT) were chosen to measure the dynamic load responses of the highly modified asphalt pavement and the subgrade within the APLF. Strain gages were installed to measure the horizontal strains that occur at the base of the fatigue and the intermediate layers. Thermocouples were then installed throughout the entire depth of the pavement in each test section to monitor the internal temperatures during testing. The LVDTs were used to observe the vertical deflections of the subgrade and the asphalt pavement structure while dynamic wheel loading occurred. Upon completion of selecting the gages, an AutoCAD document was created as a reference. An example of the instrumentation for test lane A can be seen in Figure 3.2.

Before gages were installed in the APLF, a 6 in (15.2 cm) layer of crushed 304 aggregate base was placed, leveled, and compacted on top of the existing subgrade. Following compaction, the grid layout designed using AutoCAD was implemented inside the APLF.

Four test lanes were measured to size and the centerlines were marked with spray paint. From previous research studies performed in the APLF, it was decided the first strain gage in the bottom of the fatigue layer would be placed along the centerline of each test section 6 ft (1.8 m) from the concrete platform on the south end of the facility. At this distance the initial balancing of the loads prior to the motion of the wheel would have dissipated enough that the possibility of false readings from the initial loading of the wheel would be eliminated.

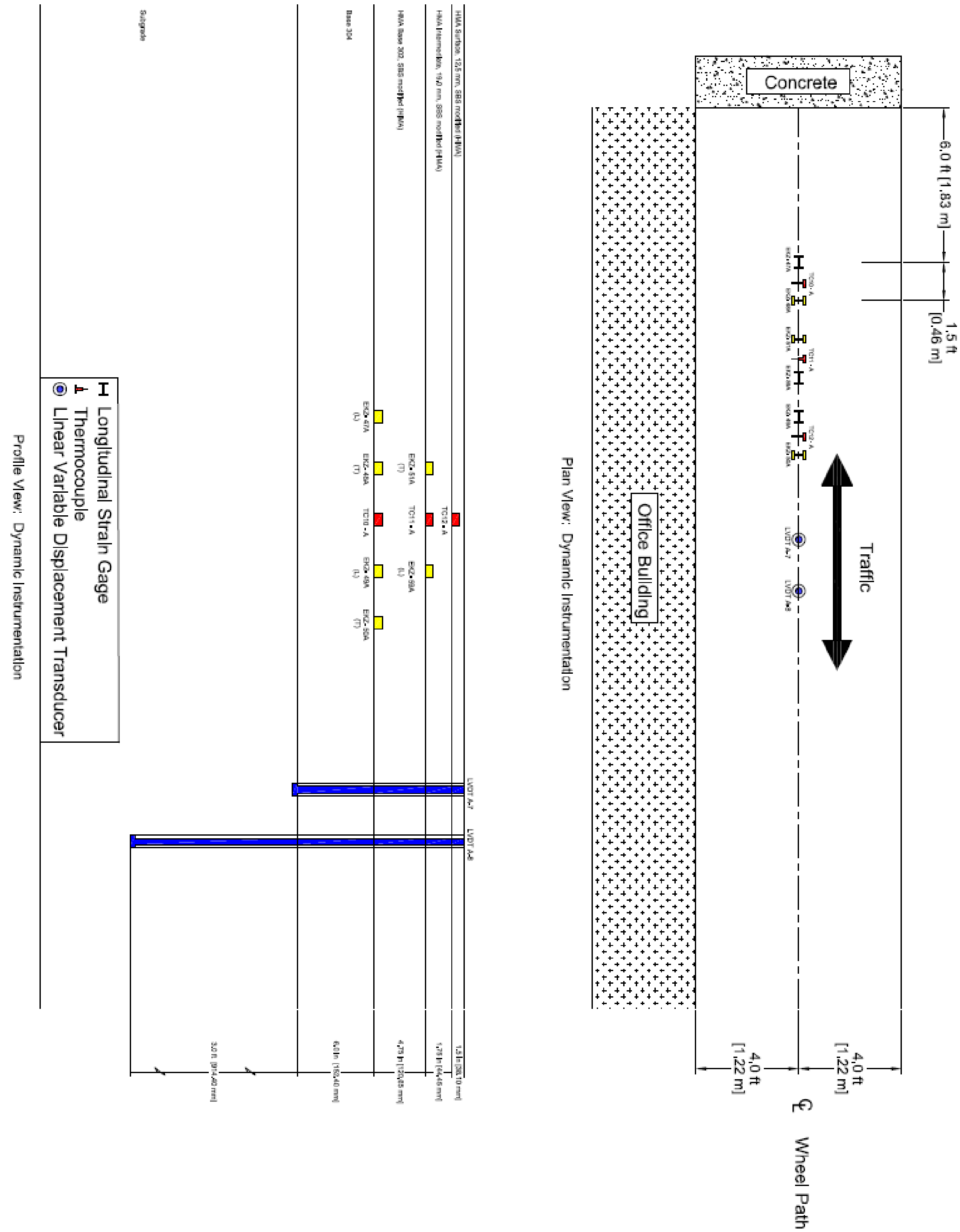

Figure 3.2 Gage Layout

3.2.1 Strain Gages Installation

A total of 24 KM-100HAS strain gages (6 per lane) were installed to measure horizontal pavement strains. The KM-100HAS strain gage designed by Tokyo Sokki Kenkyujo, has two reinforcing bars that allow the asphalt to securely adhere the gage to the pavement. Each gage has a resistance of 350 Ω in a full bridge configuration connected to terminal boards using lead wires.

Using the KM-100HAS, the pavement strains were measured in the longitudinal and transverse directions at the bottom of the AC Base and intermediate layers of each test section. The bottom of the AC Base, where bottom-up cracking commonly occurs in asphalt pavements, was chosen to have a total of 4 gages (2 in the longitudinal, 2 in transverse) to accurately monitor responses. As previously stated, the first strain gage was placed along the centerline of the lane at a distance of 6 feet (1.8 m) from the concrete platform in a longitudinal direction. To allow for substantial areal coverage, each gage was offset 1.5 feet (0.46 m) down the length of the test section along the centerline. In addition, ensuing strain gages would be placed in alternating longitudinal and transverse directions. The remaining two strain gages would be placed at the bottom of the intermediate layer. The first gage of the intermediate layer would be measured 7.5 feet (2.3 m) from the concrete platform along the same centerline used for the base layer gages. This gage would be placed in the same direction as the gage in the AC Base layer in order to properly compare the strain readings between these two layers. The sixth strain gage was offset 1.5 feet (0.46 m) from the prior gage and installed such that comparisons could be made to the third strain gage in the AC Base layer. Each subsequent test section follows this layout.

In order to ensure accurate readings from any gage, proper installation procedures must be followed. The placement and orientation of the strain gages were selected to provide substantial information at the bottom of the AC base and intermediate layers in each test section. To safeguard the strain gages from unintentional damages and movement that may occur as a result of the asphalt paver, hand installation was necessary. Asphalt was taken directly from the paver and used during installation. The asphalt was spread under and around the gage in a thin layer less than one inch (2.54 cm) thick. The strain gage was then placed on top of the asphalt in the correct direction that was previously decided for that position of the gage. Once in place, the gage was covered with more asphalt from the paver and lightly compacted to further ensure no damages or movement of the gage from the paver. This installation process was used for both layers in the asphalt pavement and the installation of the strain gages in the bottom of the AC base can be seen in the following figure.

Figure 3.3: AC Base Layer Strain Gage Installation

3.2.2 Thermocouple Installation

A total of twelve T-22N-.75E(T)9A192 thermocouples (3 per lane) were used to measure temperatures within the test section pavements. This specific type of sensor was known to effectively work over the target range of temperatures decided upon prior to construction in the APLF. Thermocouples work on the principal of thermoelectricity between two different metals. As the two metals experience a change in temperatures, a voltage is created that can be interpreted into temperature readings. In order to precisely interpret the temperatures throughout the test section pavements within the APLF a CR7 data logger was used.

Amongst the twelve thermocouples within the asphalt pavement, one thermocouple was used to measure the air temperature within the facility during dynamic testing. The temperature was monitored throughout the entire depth of the pavement by having one thermocouple in the bottom of each layer of the test section. The installation process of the thermocouples was the same as previously discussed in the strain gage section of this report; however, the location was chosen to be 8.25 feet (2.5 m) from the concrete platform along the centerline of the test section. This location was chosen to be in the center of the strain gage configuration and can be seen in the following figure.

Figure 3.4 Thermocouple atop 304 Aggregate Base

3.2.3 Linear Variable Differential Transformer (LVDT) Installation

Two Linear Variable Differential Transformers (LVDTs) at a total of 8 locations (2 per lane) were used to measure vertical pavement deflection and subgrade deflection in the APLF research. The two LVDT's used were GHSD-750-250 spring loaded type and were purchased through AST Macro Sensors. The LVDT's have a precalibrated output that ranges from 0 to ±10 V and have a diameter of 0.75 in (19.05 mm)

The LVDT installation used a process similar to the strain gage instrumentation. The LVDT installation began before any asphalt was placed inside the facility. As previously discussed in Section 3.3, each of the test sections was first developed using AutoCAD and then implemented for use within the APLF. Using the corner of the south concrete platform closest to the office as a reference point, the centerlines of each test section was found. Once the centerline of each test section was marked on each side of the concrete platform, a chalk line was used to form a straight line on the densely graded aggregate base (DGAB). From the south concrete platform two LVDT markers were sprayed on the DGAB at 12 feet (3.6 m) and 13.5 feet (4.1 m) for each test lane. At the 12 foot (3.6 m) mark, holes were excavated down to the subgrade where a shallow LVDT steel plate was placed, as shown in Figure 3.5. Holes were bored at the 13.5 feet (4.1 m) marker to a depth of 3 feet (0.91 m) into the subgrade to install deep rods to measure subgrade deflections. To ensure the hole would not collapse during construction a PVC pipe was installed into the hole.

Upon completion of placing the asphalt pavements, the LVDT holes were located and marked using the reference point previously discussed. The pavement marks were then cored to the top of the PVC piping and the LVDT steel plate. Rod extensions were attached to the shallow plates, while the deep rods were rammed into the subgrade. Next, LVDT casings were screwed and epoxied into place; such that, the casings would sit flush with the surface layer of the test sections. To ensure accurate results, the same two LVDT's were used in each test section and would be used to measure the same depth at each location on the test pavements.

Figure 3.5 LVDT Shallow Subgrade Base Plate

3.2.4 MegaDAC

Throughout the experiment, responses from the strain gages, LVDTs, and thermocouples were recorded at a rate of 1200 samples per second using a 82 channel megadac data acquisition system. Ribbon cables were connected from CB808 Terminal Boards and the CR7 data logger to the acquisition systems. Real-time measurements could be seen using the Test Control Software (TCS). To limit the amount of samples being recorded, a trip laser that communicated with the TCS system was used to initiate and terminate data collection. The trip laser was placed 6 feet (1.8 m) before the first gage in the pavement and after the last gage in the pavement.

3.2.5 Profilometer Instrumentation

For the APLF project, a rolling wheel profiler was used to measure surface rutting across the 4 test sections. Rutting, next to cracking, is one of the most common distresses an asphalt pavement will endure over its entire lifespan. For this purpose, surface profiles were taken over each test section to analyze the effectiveness of varying thickness of the new HiMA. This profiler, developed by ORITE, consists of a 10 foot (3 m) long track that allows a wheel to measure elevations to 5 mil accuracy at 0.5 inch increments (Sargand et al., 2009). The rolling wheel profilometer can be seen in the following figure.

Figure 3.6 Rolling Wheel Profiler

From previous research performed in the APLF, it was suggested the profilometer be rotated from the horizontal to minimize the effects of rutting in other test lanes on the elevation of the profiler supports as well as to allow more data points to be collected.

The rolling distance of the wheel was measured to be 9.33 feet (2.84 m); therefore, since the lanes were 8 feet (2.5 m) wide, an optimum angle of 31° was chosen. To ensure rut measurements were taken from the same locations, metal washers were epoxied to the surface of each test pavement at the location where each support contacted the asphalt. The total distance between each leg was measured and an optimum layout was created using AutoCAD such that four profiles were taken at equally spaced intervals along each test section. In order to compensate for the starting location of the profiler wheel, which is in front of the legs, profiler positions on Lane C and Lane D were a mirror image of those on Lane A and Lane B. The profilometer layout can be seen in Figure 3.7.

As agreed upon between ODOT and ORITE, the strains and displacement of the test pavements caused by the dynamic wheel loadings would be analyzed as well as the susceptibility of pavement rutting. Rutting was measured initially and again after 100, 300, 1000, 3000, and 10,000 wheel passes per test section respectively. The pavement profiles were recorded using a Windows DOS program created by ORITE.

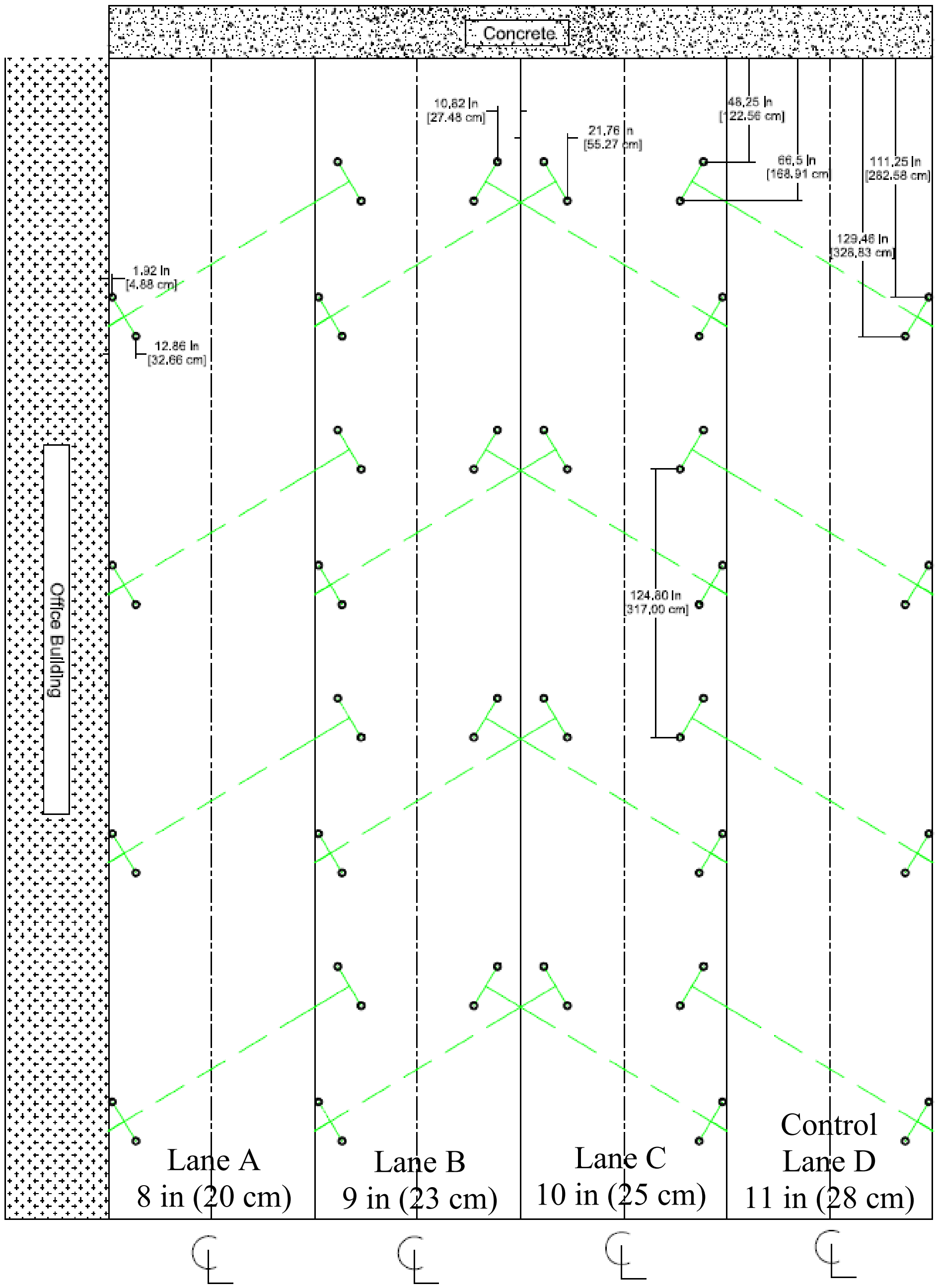

Figure 3.7 Overhead View of Test Pavements in APLF Showing Placement of Profilometer

3.2.6 Wandering Effect

From past research, it has been shown that the highest amount of strains generated on the APLF test pavements occurs when the wheel is centered over the gages; however, this worst case scenario rarely occurs for in-use pavements. Utilizing the APLF ability with tire offsets, the effects of tire wandering was analyzed in order to ensure that a test section would sustain perpetual design at four different offsets. The four tire offsets were chosen at 0 in, -2 in (-5 cm), -6 in (-15 cm), and -12 in (-30 cm) from the centerline. A dual wide-based tire was used during this study with each tire width measuring 9.5 in (24.1 cm) in width and having a gap distance between the tires measuring 4.5 in (11.4 cm). The 0 inch offset refers to the wheel being spaced equidistantly along the centerline of each test section. The negative sign symbolizes that the wheel is being shifted laterally in one direction along the centerline at the numerical distance following the sign. These locations can be seen in the following figure.

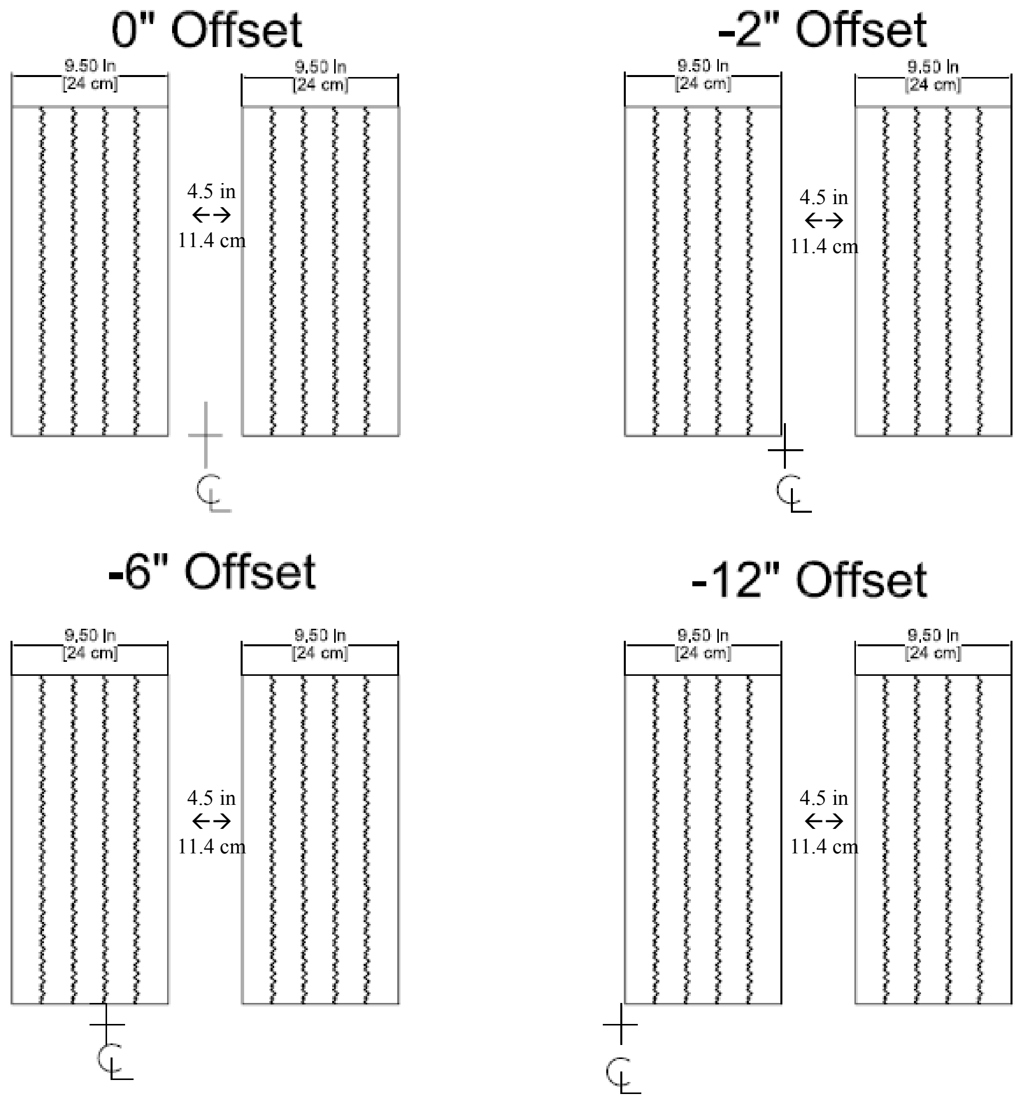

Figure 3.8 Lateral Tire Offset

3.3 Estimating the Fatigue Endurance Limit

Designing a perpetual pavement can be accomplished by eliminating detrimental pavement distresses such as bottom-up fatigue cracking and rutting. Despite having many different implemented perpetual pavement designs, the design premise for these pavements remains unchanged. This perpetual pavement design, whether built of three or four asphalt layers, includes a top layer designed to resist rutting and tire wear, an intermediate layer that also resists rutting, and a rich asphalt bottom layer designed to resist fatigue cracking, known as the fatigue resistance layer (FRL). The thicknesses of the layers are increased such that the strain at the bottom of the FRL, where it contacts the dense graded aggregate base (DGAB) never exceeds a specified value of the longitudinal tensile strain, called the "fatigue endurance limit".

Using the results of the dynamic modulus test to estimate the initial flexural stiffness (E_0), a fatigue endurance limit can be found for each mix. The NCHRP project 9-44A included laboratory testing programs, which lead to the development of a model that estimates the fatigue endurance limit based on results of the beam fatigue test (Witczak et al., 2013). In this model, the Stiffness Ratio (*SR*) was calculated based on applied tensile strain, rest periods, number of loading cycles, and the initial flexural stiffness found from the results of beam fatigue testing. The endurance limit of an asphalt mix can be determined by setting the Stiffness Ratio equal to one and solving for the tensile strain. This equation derived by Witczak et al., (2013) can be seen again in section 2.3 of this report.

Findings from the NCHRP 9-44A report included a sensitivity study which concluded that the number of loading cycles "*N"* has a negligible effect on the Stiffness Ratio. With loading cycles having little effect on the ratio, "N" is set to 200,000 cycles for the APLF analysis, as recommended by the NCHRP 9-44A researchers (Witczak et al., 2013). However, the study found that Rest Period (*RP*) had a major influence on the endurance limit up to a period of 5 seconds. Once the rest period reached or exceeded 5 seconds, the endurance limits started to become very similar.

3.3.1 Effect of the Initial Flexural Stiffness

In addition to rest periods, flexural stiffness of a mix has an effect on the endurance limit. Typically, as the stiffness decreases within an asphalt mix, the endurance limit increases due to the material becoming more flexible and ductile; whereas, when the stiffness increases, the endurance limit decreases because the mixture becomes more brittle. The value of the dynamic modulus and flexural stiffness for a mix is dependent on the temperature and frequency. At higher temperatures the dynamic modulus has a lower value opposed to testing conducted at lower temperatures at the same frequency. Relationships between the dynamic modulus and temperature for each base layer mix will be determined to estimate the value of the dynamic modulus at a particular test temperature.

In an attempt to estimate the flexural stiffness for a mix without using the four point beam bending test, the dynamic modulus was used to estimate the flexural stiffness; however, estimating the flexural stiffness based on the dynamic modulus is somewhat controversial. The NCHRP Design Guide assumes the dynamic modulus is equal to the initial flexural stiffness, whereas Kansas researchers found the dynamic modulus is two times the value of the initial flexural stiffness (Romanoschi, et al, 2006). In addition, Romanoschi, et al. (2006), stated to produce these results a 10 Hz frequency must be used when testing for the dynamic modulus. Both assumptions will be used to compare the various endurance limits for this analysis ($E_0 = E^*$ and $E_0 = E^*/2$) at a loading frequency of 10 Hz for the dynamic modulus.

3.4 Test Section Design

Four asphalt test sections with varying AC Base layer thicknesses were used in the APLF for dynamic load testing. Of the four sections, three test sections used a HiMA AC Base layer produced by Kraton Polymers. Each test section was built above a 6 in (15.24 cm) DGAB that rested on an 18 in (45.72 cm) cement stabilized subgrade. The following table shows the thickness for the AC layers for the Highly Modified Asphalt (HiMA) and controlled pavement sections in the APLF, as provided by Shelly Company at the time of paving.

Table 3.1 APLF Test Section Layer Thickness

Layer	ODOT Item	Layer Thickness for Each Section							
		Lane A (HiMA)		Lane B (HiMA)		Lane C (HiMA)		Lane D (Control)	
		(in)	(cm)	(in)	(cm)	(in)	(cm)	(in)	(cm)
Surface	442	1.50	3.81	1.50	3.81	1.50	3.81	1.50	3.81
Intermediate	442	1.75	4.45	1.75	4.45	1.75	4.45	1.75	4.45
AC Base	302	4.75	12.07	5.75	14.61	6.75	17.15	7.75	19.69
Total AC	**-**	**8.00**	**20.33**	**9.00**	**22.87**	**10.00**	**25.41**	**11.00**	**27.95**
Aggregate Base	304	6.00	15.24	6.00	15.24	6.00	15.24	6.00	15.24
Cement Stabilized Subgrade	206	18.00	45.72	18.00	45.72	18.00	45.72	18.00	45.72
Subgrade (type)	-	A6-A7		A6-A7		A6-A7		A6-A7	

3.5 Laboratory Testing

3.5.1 Rice Test

To determine the volumetric and mix design properties of the asphalt mixes used in this project, a Rice test was conducted to compute the theoretical maximum specific gravity (G_{mm}) and the density of each asphalt mix. Tests of the AC mixes were performed in accordance to AASHTO T 209. Prior to testing, each AC mix was spread out and broken up to remove large clumps of the materials. Once broken apart the samples were weighed and placed into a water filled shaker table with a vacuum pump attached. The samples were then tested to meet the requirements given by AASHTO T 209. The mixes for this project were tested and provided by Shelly Company at the time of paving. The properties of each AC mix design can be seen in Table 3.2. The HiMA binder properties (Table 3.3) were taken from the NCAT report on High Polymer Mixtures (Timm et al., 2013), along with control binder information from Division of Construction Management, Office of Materials Management, Asphalt Materials Section.

Table 3.2 AC Mix Design and Volumetrics for HiMA and Control Materials in APLF

Layer	Surface	Intermediate	AC Base-Kraton	AC Base-Control
Mix	442	442	302	302
Gradation				
2" (50.8 mm)	100	100	100	100
1 1/2" (38 mm)	100	100	100	100
1" (25.4 mm)	100	100	87	87
3/4" (19 mm)	100	96	78	78
1/2" (12.5 mm)	100	80	68	68
3/8" (9.5 mm)	93	69	58	58
#4 (4.75 mm)	57	48	39	39
#8 (2.36 mm)	38	35	28	28
#16 (1.18 mm)	27	26	22	22
#30 (0.600 mm)	19	18	16	16
#50 (0.300 mm)	11	11	9	9
#100 (0.150 mm)	7	7	6	6
#200 (0.075 mm)	4.8	4.9	4.3	4.3
Agg. Blend G_{sb}	2.393	2.636	2.646	2.646
G_{mm}	2.440	2.496	2.480	2.485
% Binder Content	5.7	4.4	4.4	4.3
% Virgin Binder	5.0	3.2	2.7	2.5
Asphalt Binder	PG 88-22	PG 88-22	PG 88-22	PG 64-22
Design, Air Voids (%)	3.5	4.0	4.0	4.0
F/A	0.8	1.1	-	-
RAP %	15	25	35	35

Table 3.3 APLF Test Section Binder Properties (10 rad/s)

PG Grade	Phase Angle	Test Temperature		G*	
	(degrees)	(°F)	(°C)	(Pa)	(psi)
88-22 (HiMA) (Timm et al., 2013)	48.9	212.0	100	800	0.12
64-22 (Control)	86.7	147.2	64	1408	0.20

CHAPTER 4: APLF TESTING PAVEMENT RESPONSES

Dynamic load testing was conducted in the APLF on the highly modified asphalt mix designed by Kraton Polymers containing 7.5% polymer content during the months of May through September 2014. Testing was performed at two temperatures (70°F (21.1°C) and 100°F (37.8°C)). Upon completion of 10,000 passes on all lanes at 70°F (21.1°C), the temperature was increased to 100°F (37.8°C). The temperature was then allowed to stabilize throughout the pavement thickness. Next, 10,000 passes were applied to all lanes at the higher temperature. Profiles were taken to measure rutting of each test section prior to loading and upon completion of 100, 300, 1000, 3000, and 10,000 passes of a 9000 lb (40 kN) load. After completion of 100, 3000, and 10,000 passes, the lead wires were attached to the LVDTs and twelve passes of three wheel loads (6000 lb (27 kN), 9000 lb (40 kN) and 12,000 lb (53 kN)), at various offsets to the centerline of the lane, were applied to analyze the test section's pavement response. The tire travelled at an approximate speed of 5 mph (8 km/h). Longitudinal strains in the base layer of each test section were compared to calculated endurance limits to determine which sections met the perpetual design concept. Deflections were measured at the bottom of the 304 aggregate base and 36 in (91 cm) into the subgrade.

4.1 Strain Responses in the HiMA Pavement

During testing, strain responses were measured in the same direction as traffic (the rolling load wheel), or called the "longitudinal" direction, and in the perpendicular or "transverse" direction. Strains found in the longitudinal direction initially produced compressive strains as the wheel approached the gage as well as after the wheel passed over the gage. However, while the wheel was over the gage, the strains in the pavement switched from compressive to tensile strains. Figure 4.1 shows the longitudinal strains recorded for 8 in (20 cm) pavement (Lane A) during a 12 kip (53 kN) loading while the entire pavement was kept at 70°F (21.1°C).

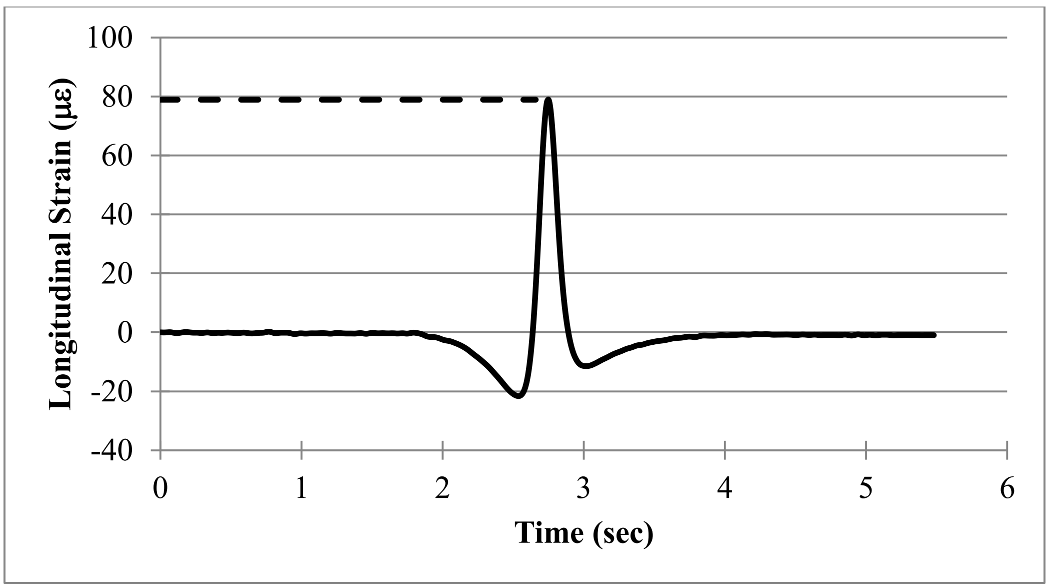

Figure 4.1 Longitudinal Strain at bottom of AC Base in Lane A, 70°F (21.1°C), 12 kip (53 kN) load

As seen in Figure 4.1, the maximum longitudinal strain produced for the 8 inch lane was found to be 79 με and is represented by the dashed line. The compressive strains in the pavement are represented by the negative values in the figure, whereas the positive values are representative of the tensile strains. The figure shows that as the wheel approaches the longitudinal strain gage, the pavement initially starts to go into compression but as the wheel continues over the gage the pavement changes to tension briefly before returning to compression.

Strains measured in the transverse direction caused the pavement to act in both compression and tension depending on the depth within the pavement. Transverse strains measured at the bottom of the AC base produced tensile strains, while strains measured at the bottom of the intermediate layer produced compressive strains. Figure 4.2 shows the transverse strains recorded for the 10 in (25 cm) pavement (Lane C) during a 12 kip (53 kN) load, while the full depth of the pavement structure was maintained at 70°F (21.1°C).

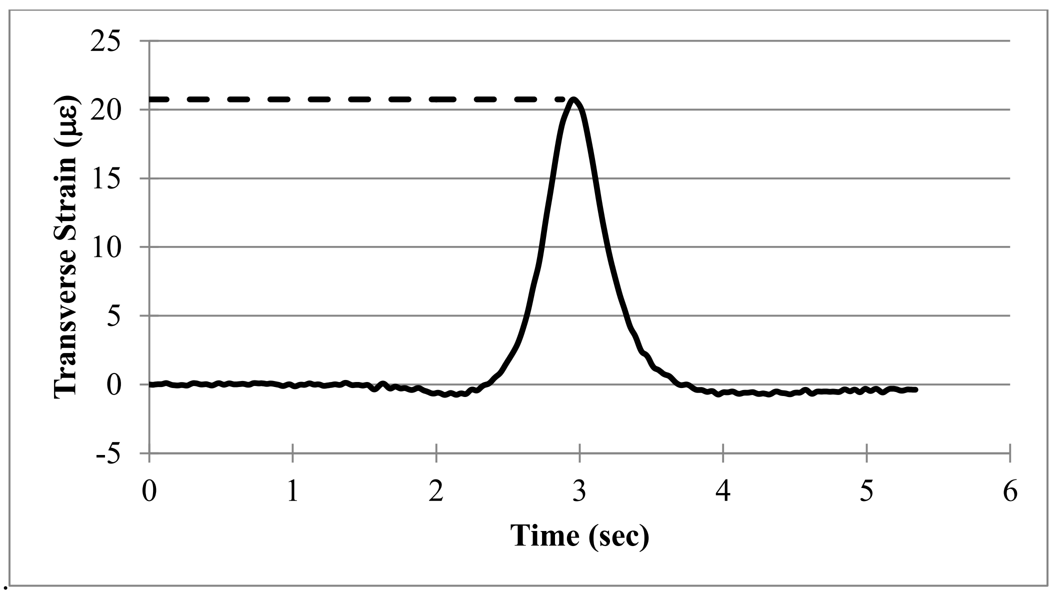

Figure 4.2 Transverse Strain at bottom of AC Base in Lane C, 70°F (21.1°C), 12 kip (53 kN) load

4.2 Longitudinal Strain Caused by Adjusted Loadings in AC Base Layers

As discussed earlier in Chapter 2, the concept of perpetual pavement design is the belief that if strains are kept below a certain limit in the bottom of the AC base layer the life expectancy of the asphalt pavement increases.

The 8 in (20 cm) test section, Lane A, produced the highest longitudinal strains in the AC base during dynamic testing in the APLF. The following table shows the average and maximum longitudinal strains found at "0" offset in Lane A (8 in (20 cm)), Lane B (9 in (23 cm)), Lane C (10 in (25 cm)), and the control Lane D (11 in (28 cm)) produced during testing in the 70° F (21.1°C) and the 100°F (37.8°C) temperatures under three wheel loads of 6000 lb (27 kN), 9000 lb (40 kN), and 12,000 lb (53 kN). Table 4.1 shows that the highest maximum strains of 79 $\mu\varepsilon$ and 113 $\mu\varepsilon$ were produced under the 12,000 lb (53 kN) wheel loads for both temperatures on the thinnest (8 in (20 cm)) test section. The results show the 10 in (25 cm) section (Lane C) using the HiMA, produced strains lower than the 11 in (28 cm) control (Lane D) for testing at 70° F (21.1°C) and yielded similar longitudinal strains at 100°F (37.8°C).

Table 4.1 Average and Maximum Longitudinal Strains in Base Layer (με)

Lane	AC thickness (in)	AC thickness (cm)	Load (lbs (kN)) 6000 (27) Avg	6000 (27) Max	9000 (40) Avg	9000 (40) Max	12000 (53) Avg	12000 (53) Max
70° F (21.1° C)								
A	**8**	**20**	35	43	54	61	70	79
B	**9**	**23**	31	36	48	54	62	69
C	**10**	**25**	21	24	35	39	46	51
D	**11**	**28**	27	43	40	55	52	67
100° F (37.8° C)								
A	**8**	**20**	62	66	89	93	106	113
B	**9**	**23**	41	46	63	73	79	83
C	**10**	**25**	34	44	50	56	61	67
D	**11**	**28**	27	34	43	56	56	73

Figure 4.3 is a plot of average maximum longitudinal strains versus the three wheel loads applied during testing at 70° F (21.1°C), and the results of testing completed at 100°F (37.8°C) can be seen in Figure 4.4. As seen in the table as well as the following Figure 4.3 and Figure 4.4, typically the 11 in (28 cm) control lane (Lane D) produced the lowest average maximum longitudinal strains in the AC base layer at 100°F (37.8°C) under all three loads, while at 70° F (21.1°C), the 10 in (25 cm) HiMA lane (Lane C) produced the lowest average maximum longitudinal strains.

As seen in Figure 4.3, longitudinal strains in the 10 in (25 cm) section (Lane C) were less than those in the 11 in (28 cm) control section (Lane D) during testing conducted at 70°F (21.1°C). However, the 8 inch and 9 inch sections both produced average maximum longitudinal strains higher than strains in the AC base of the 11 in (28 cm) control lane.

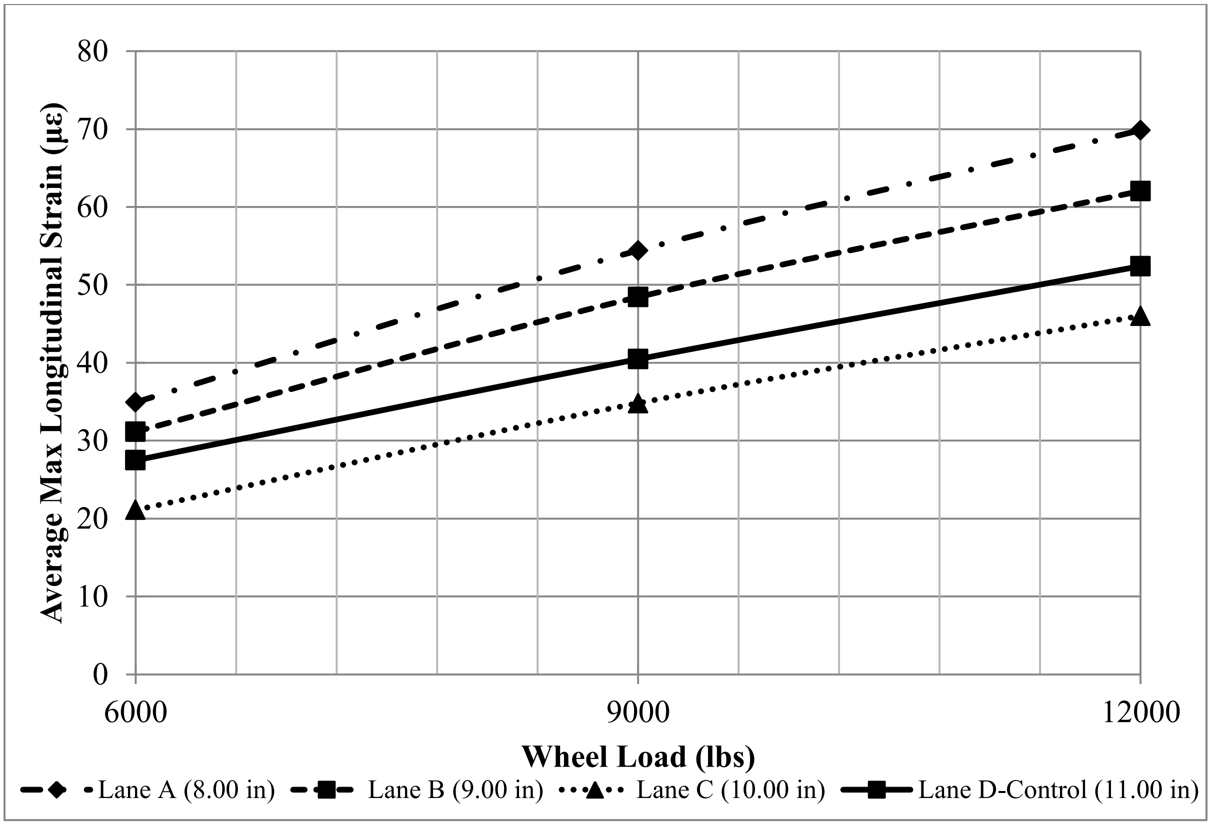

Figure 4.3 Average Max Longitudinal Strains for Test Sections at 70℉ (21.1℃)

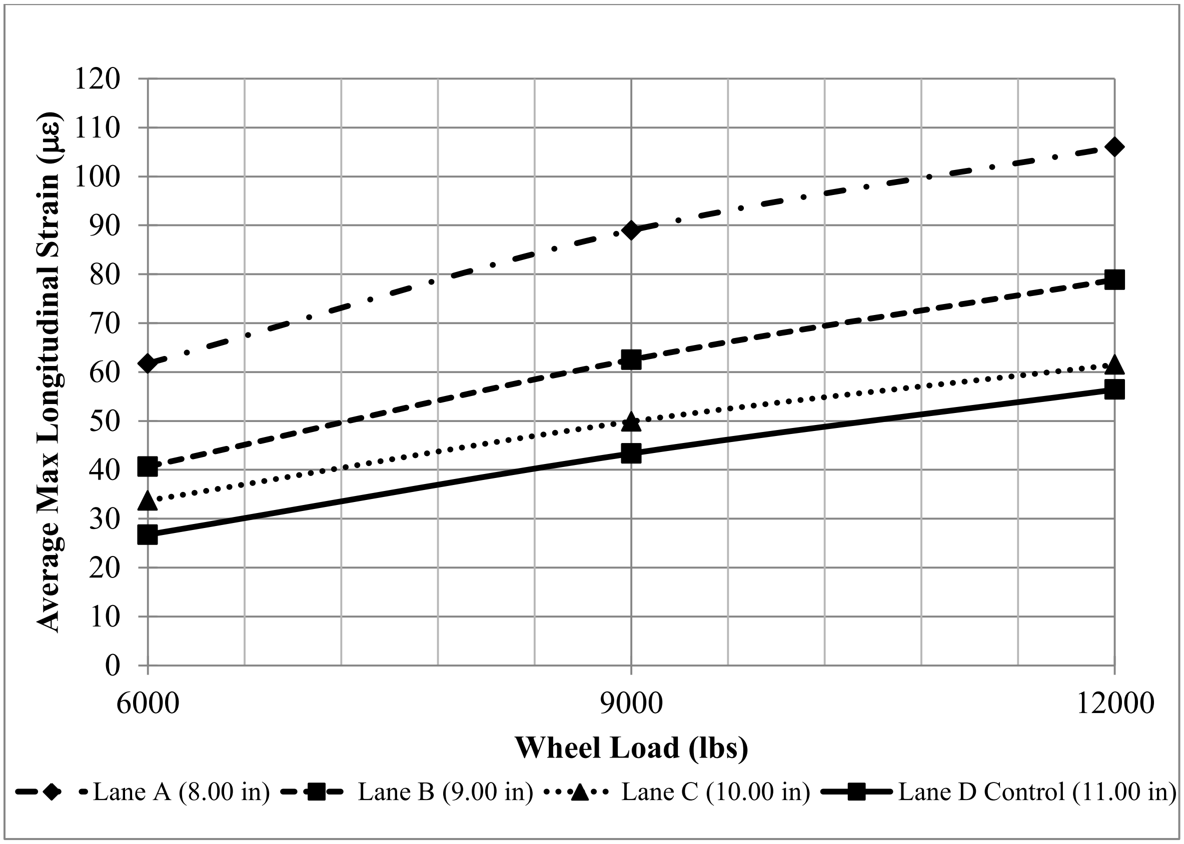

Figure 4.4 Average Max Longitudinal Strains for Test Sections at 100°F (37.8°C)

At 100°F (37.8°C), once again Lane A and Lane B produced higher longitudinal strains than the other two test sections. As seen in Figure 4.4, the effects of temperature on the 8 inch section caused much higher strains to be produced when being compared to the 9 inch and 10 inch HiMA sections and the 11 inch control section.

4.3 Strain Comparison Caused by Adjusted Loadings in AC Base Layers

In addition to longitudinal strains, transverse strains were recorded for each test section at the bottom of the AC base layer to allow for an added comparison to be made for each pavement design. Throughout testing it was discovered that the longitudinal strains were larger than the transverse strains, and that the largest strains were produced under the heaviest loading of 12 kip (53 kN). The following table shows the average maximum transverse and longitudinal strains produced for each test section under the three loadings used in the APLF testing.

Table 4.2 Longitudinal and Transverse Strains in the AC Base Layers at 70°F (21.1°C)

Lane	**Load (lbs (kN))**					
	6000 (27)		**9000 (40)**		**12000 (53)**	
	Trans.	***Long.***	***Trans.***	***Long.***	***Trans.***	***Long.***
A	9	43	12	61	16	79
B	10	36	13	54	17	69
C	12	24	18	39	24	51
D	29	43	35	55	41	67

Using the measured strains from Table 4.2, the transverse strains could be compared to the longitudinal strains under each load condition. These comparisons can be seen in the following table.

Table 4.3 Percentage of Transverse Strain to Longitudinal Strain in Base Layer at 70°F (21.1°C)

Lane	**Pavement Thickness**		**Load (lbs (kN))**		
	in	**cm**	**6000 (27)**	**9000 (40)**	**12000 (53)**
A	8	20	21%	20%	21%
B	9	23	27%	25%	25%
C	10	25	48%	47%	47%
D	11	28	67%	63%	61%

Results from Table 4.3 suggest that the percentage of transverse strains compared to longitudinal strains created in each pavement react similarly regardless of the load magnitude; however, the results suggest that the depth of the pavement can be a contributor to this strain relationship. To analyze this trend further the Figure 4.5 was created using the average transfer percentage of the three loadings from APLF testing and plotted against the depths of each test section.

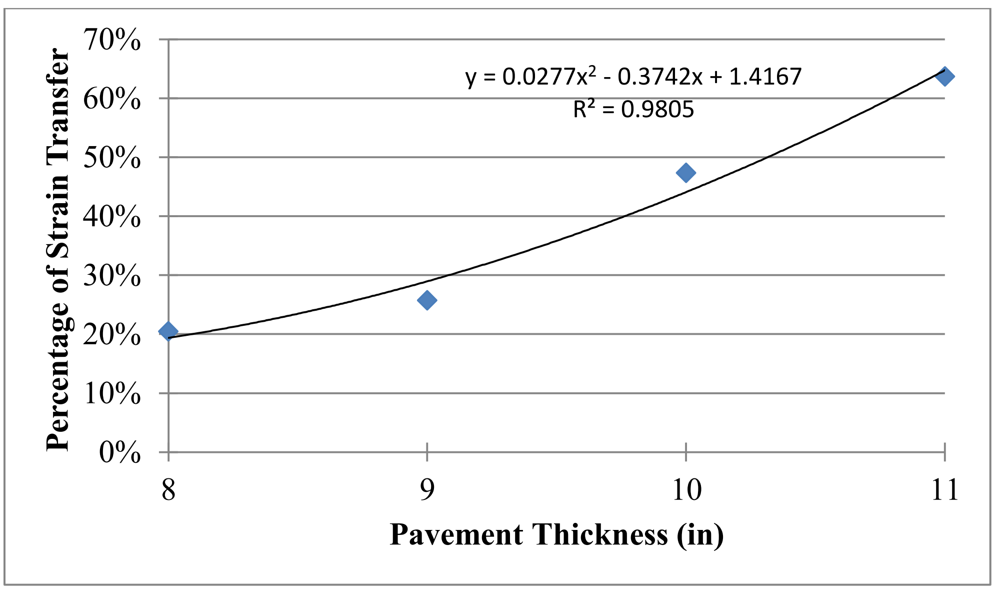

Figure 4.5 Percentage of Strain Transfer Compared to Pavement Thickness

Using a trendline, a parabolic model could be created to estimate the percentage of transverse to longitudinal strains for various pavement thicknesses with a stabilized subgrade. This model suggests that thicker pavements would eventually produce transverse strains larger than longitudinal strains regardless of loading. This phenomenon was noted by Scheer (2013) on a 13 inch asphalt pavement with a chemically stabilized subgrade in Delaware, Ohio. In his report he found that the transverse strains measured on this section produced larger than the longitudinal direction. Using the model created from Figure 4.5 and inputting the depth of 13 inches produces a percentage of 123% was calculated; this value agrees with Scheer's findings.

4.4 Strain Influence Caused by Temperature in AC Base Layer

To analyze the effect of how temperature affected the HiMA pavements the entire pavement from surface to base was increased and maintained from 70° F to 100° F. It was expected that the increase in temperature would cause an increase in the amount of strains generated in the HiMA Base. The following table shows the average longitudinal strain increase that occurred within each test section in the AC base layers under the 6,000 lb (27 kN), 9,000 lb (40 kN), and 12,000 lb (53 kN) wheel loads.

Table 4.4 Percent Increase in Longitudinal Strains Due to Temperature Increase from 70°F (21.1°C) to 100°F (37.8°C)

Lane	**Load (lbs (kN))**		
	6000 (27)	**9000 (40)**	**12000 (53)**
A	177%	164%	152%
B	131%	129%	127%
C	160%	143%	134%
D	97%	107%	108%

Surprisingly, results showed that in the three lanes where the HiMA was present, the increase in temperature caused the longitudinal strains produced by the heavier loadings act more similar to the same loadings at the lower temperature. However, the 11 inch control test section, Lane D, produced an increasing trend opposite of the other three lanes. As mentioned in Section 4.2 and seen from Table 4.2, the 8 inch section, Lane A, was the most susceptible to the temperature change. Figure 4.6 shows the effect of the increase in temperature under the same wheel loadings by comparing the average maximum longitudinal strains produced by Lane A for both the 70°F (21.1°C) and the 100°F (37.8°C) temperatures.

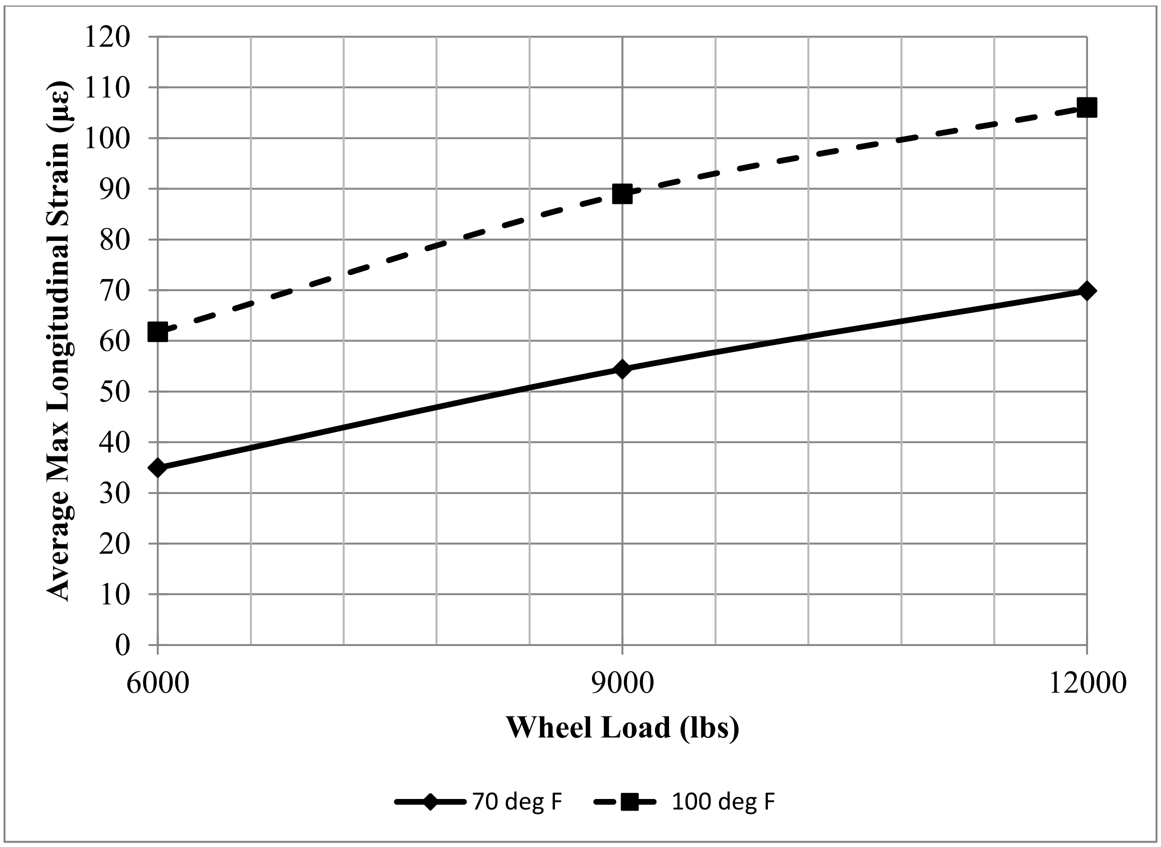

Figure 4.6 Comparison of Average Max Longitudinal Strains Produced in HiMA Base for Lane A

4.5 Wheel Wander Analysis in APLF

Longitudinal strains in the AC base were measured under three loadings 6,000 lb (27 kN), 9,000 lb (40 kN), and 12,000 lb (53 kN) at locations 0 in, -2 in (-5 cm), -6 in (-

15 cm), and -12 in (-30 cm) from the centerline of each test section in the APLF to analyze the strain influence caused by wheel wandering. The average longitudinal strain measured in each test section under the various loads and offsets mentioned prior are shown for 70°F (21.1°C) in Table 4.5 and for 100°F (37.8°C) in Table 4.6.

Table 4.5 Average Longitudinal Strain with Sway Analysis in AC Base Layers at 70°F (21.1°C)

Wheel Load		**Lateral Shift**		**Average Longitudinal Strain (με)**			
(lb)	**(kN)**	**(in)**	**(mm)**	**Lane A**	**Lane B**	**Lane C**	**Land D**
6000	**27**	0	0	35	31	21	27
		-2	-51	36	32	22	28
		-6	-152	38	35	22	28
		-12	-305	28	30	18	24
9000	**40**	0	0	54	48	35	40
		-2	-51	55	49	35	41
		-6	-152	58	52	35	38
		-12	-305	44	44	29	36
12000	**53**	0	0	70	62	46	52
		-2	-51	71	63	46	54
		-6	-152	73	65	46	53
		-12	-305	57	56	39	47

Table 4.6 Average Longitudinal Strain with Sway Analysis in AC Base Layers at 100°F (37.8°C)

Wheel Load		**Lateral Shift**		**Average Longitudinal Strain (με)**			
(lb)	**(kN)**	**(in)**	**(mm)**	**Lane A**	**Lane B**	**Lane C**	**Land D**
6000	**27**	0	0	62	41	34	27
		-2	-51	62	42	33	28
		-6	-152	68	47	33	29
		-12	-305	49	41	26	24
9000	**40**	0	0	89	63	50	43
		-2	-51	89	64	49	44
		-6	-152	95	68	48	45
		-12	-305	71	57	39	37
12000	**53**	0	0	106	79	61	56
		-2	-51	107	81	61	58
		-6	-152	111	82	60	58
		-12	-305	86	69	49	49

Table 4.5 and Table 4.6 show that the maximum longitudinal strains at both temperatures occurred at an offset of -6 in (-15 cm) from the centerline for each test section; however, the increased strain produced at this distance does not significantly affect the longitudinal strain produced in the AC base layers, as seen in Figure 4.7. Figure 4.7 provides a graphical representation of the longitudinal strains produced in each test section under a 6000 lb (27 kN) load while being maintained at 100°F (37.8°C).

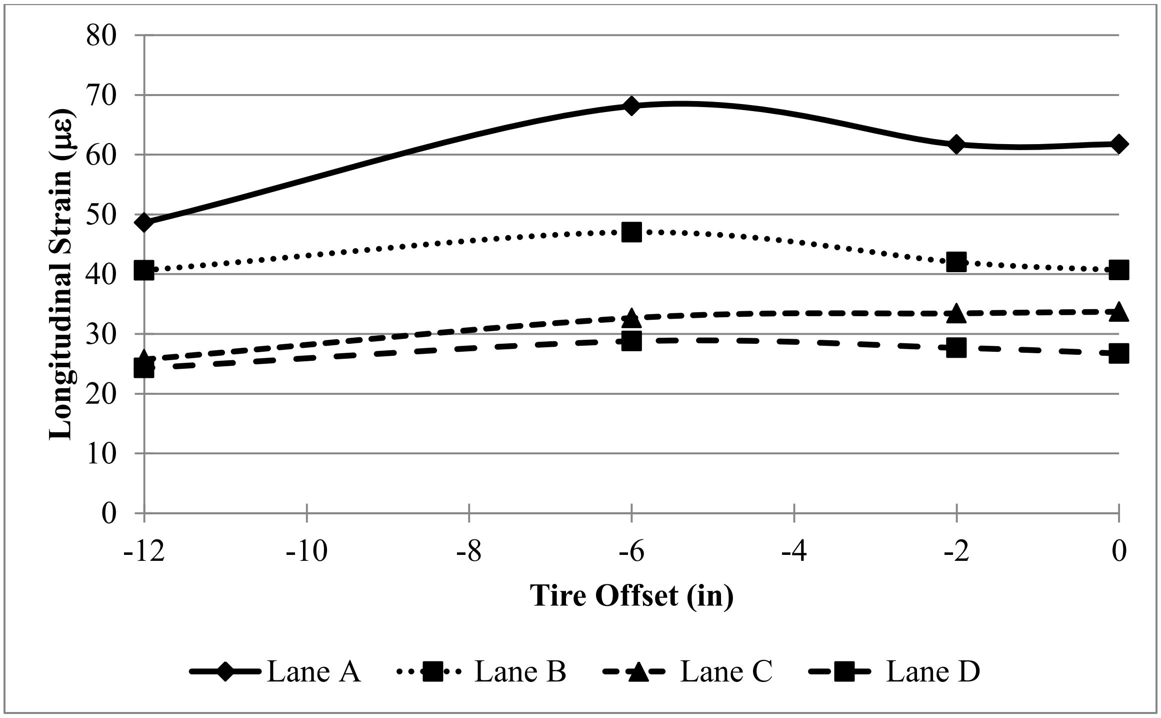

Figure 4.7 Longitudinal Strain Produced by Varying Tire Offset in APLF Test Sections

4.6 Linear Variable Differential Transformer (LVDT) Analysis in APLF

Deflections of the aggregate base and three feet into the subgrade were measured for each of the sections used during testing within the APLF. The following table shows the deflections of the test sections measured at 70°F (21.1°C) and 100°F (37.8°C)) with a wheel load of 12,000 lbs (53 kN).

Table 4.7 Average and Maximum Deflections Produced by 12,000 lb (53 kN) Wheel Load

Lane	**AC thickness**		**LVDT Aggregate Base**		**LVDT Subgrade**	
			Mils		**Mils**	
	(in)	**(cm)**	***Avg***	***Max***	***Avg***	***Max***
70° F (21.1° C)						
A	**8**	**20**	1.84	2.36	4.46	4.72
B	**9**	**23**	0.79	0.90	2.81	3.09
C	**10**	**25**	1.29	1.48	2.92	3.31
D	**11**	**28**	-	-	2.74	2.75
100°F (37.8° C)						
A	**8**	**20**	2.32	2.53	6.09	6.33
B	**9**	**23**	1.59	1.68	3.68	3.73
C	**10**	**25**	1.86	2.05	3.84	4.59
D	**11**	**28**	2.14	2.26	3.60	4.37

Table 4.7 showed that the maximum deflection of 6.33 mils occurred in the thinnest test section at 100°F (37.8°C). Results for test Lane D at 70°F (21.1°C) could not be interpreted due to gage malfunction while performing dynamic testing of this section.

4.7 Dynamic Modulus

To determine the frequency and temperature dependent viscoelastic material properties of the asphalt concrete materials used in this project, master curves were computed using laboratory data. Dynamic modulus tests of AC specimens were performed in accordance to AASHTO TP 62. Specimens were compacted during paving at the asphalt plant using the Superpave Gyratory Compactor (SGC) in accordance with AASHTO T 312. The specimens were compacted with a 7% target air void to a thickness of 165 mm (6.5 in) and a 150 mm (5.91 in) diameter. The specimens were then cut and cored to a thickness of 150 mm (5.91 in) and a diameter of 100 mm (3.94 in) to meet the size requirements given by AASHTO TP 62.

Each specimen was tested using the Simple Performance Tester (SPT) for dynamic modulus at the following temperatures in order 4.4 °C (40 °F), 21.1 °C (70 °F), 37.8 °C (100 °F), and 54.4 °C (130 °F). For each test temperature, the dynamic modulus was calculated using various loading frequencies that included: 25 Hz, 10 Hz, 5 Hz, 1 Hz, 0.5 Hz, and 0.1 Hz respectively. The dynamic modulus can be determined by the following equation:

$$|E^*| = \frac{\sigma_0}{\varepsilon_0} \qquad Eq. 3$$

Where:

$|E^*| = Dynamic\ Modulus$

$\sigma_0 = Average\ peak\ stress\ over\ the\ last\ five\ periods$

$\varepsilon_0 = Average\ peak\ strain\ over\ the\ last\ five\ periods$

The results of the dynamic modulus tests for the 442 surface mix, 442 Intermediate mix, 302 AC Base mix (with Kraton binder), and the 302 AC Base mix (control binder) for the HiMA study in the APLF are shown in the following tables:

Table 4.8 Average Dynamic Modulus of the 442 Surface Layer - HiMA

Temperature	Frequency (Hz)	Dynamic Modulus (ksi)	Dynamic Modulus (MPa)
40 °F (4.4 °C)	25	2079	14336
	10	1937	13358
	5	1816	12520
	1	1547	10669
	0.5	1424	9816
	0.1	1160	7998
70 °F (21.1 °C)	25	1116	7697
	10	976	6732
	5	872	6010
	1	653	4504
	0.5	576	3971
	0.1	411	2834
100 °F (37.8 °C)	25	535	3690
	10	440	3033
	5	377	2602
	1	252	1739
	0.5	218	1503
	0.1	142	980
130 °F (54.4 °C)	25	281	1935
	10	223	1537
	5	191	1318
	1	129	893
	0.5	113	780
	0.1	83	571

Table 4.9 Average Dynamic Modulus of the 442 Intermediate Layer - HiMA

Temperature	Frequency (Hz)	Dynamic Modulus (ksi)	Dynamic Modulus (MPa)
40 °F (4.4 °C)	25	2216	15278
	10	2073	14291
	5	1953	13466
	1	1665	11478
	0.5	1534	10576
	0.1	1243	8570
70 °F (21.1 °C)	25	1304	8994
	10	1145	7897
	5	1022	7049
	1	765	5276
	0.5	668	4606
	0.1	468	3228
100 °F (37.8 °C)	25	624	4303
	10	507	3494
	5	428	2951
	1	278	1914
	0.5	233	1604
	0.1	151	1040
130 °F (54.4 °C)	25	257	1773
	10	193	1332
	5	161	1110
	1	105	721
	0.5	90	620
	0.1	66	453

Table 4.10 Average Dynamic Modulus of the 302 AC Base with Kraton Binder - HiMA

Temperature	Frequency (Hz)	Dynamic Modulus (ksi)	Dynamic Modulus (MPa)
40 °F (4.4 °C)	25	2925	20167
	10	2769	19089
	5	2627	18112
	1	2291	15796
	0.5	2132	14702
	0.1	1775	12239
70 °F (21.1 °C)	25	1737	11975
	10	1552	10702
	5	1400	9652
	1	1070	7379
	0.5	944	6507
	0.1	670	4622
100 °F (37.8 °C)	25	882	6078
	10	733	5056
	5	628	4327
	1	416	2870
	0.5	357	2462
	0.1	238	1639
130 °F (54.4 °C)	25	377	2596
	10	290	1997
	5	248	1706
	1	162	1119
	0.5	131	906
	0.1	103	708

Table 4.11 Average Dynamic Modulus of the 302 AC Base with Control Binder - HiMA

Temperature	Frequency	Dynamic Modulus	
	(Hz)	(ksi)	(MPa)
40 °F (4.4 °C)	25	2879	19850
	10	2729	18816
	5	2581	17797
	1	2250	15514
	0.5	2089	14406
	0.1	1727	11906
70 °F (21.1 °C)	25	1710	11792
	10	1515	10445
	5	1364	9406
	1	1028	7087
	0.5	895	6170
	0.1	628	4330
100 °F (37.8 °C)	25	833	5746
	10	677	4669
	5	569	3921
	1	358	2465
	0.5	295	2031
	0.1	184	1271
130 °F (54.4 °C)	25	294	2024
	10	211	1453
	5	171	1176
	1	105	727
	0.5	88	606
	0.1	64	439

To further determine the viscoelastic material properties of the asphalt concrete materials, a shift factor must be determined in order to build a master curve. The shift factor a(T), is calculated by finding the best-fit, second-order polynomial when plotting the shift factor against the test temperature. The following equation describes this relationship:

$$\log a(T) = C_1 + C_2 * T + C_3 * T^2 \qquad Eq. 4$$

Where:

$\log a(T) = Shift\ Factor$

$T = Actual\ Test\ Temperature$

$C_1, C_2, C_3 = Regression\ Coefficients$

The dynamic modulus is determined at various temperatures and is plotted against frequency. The data is then shifted to a reference temperature of 21.1 °C (70 °F) to form the master curve for the mix. This parallel-shift is performed by determining the reduced frequency for each test frequency and temperature based on the reference temperature. The following equation is used to determine the reduced frequency:

$$\log f_r = \log f + \log a(T) \qquad Eq. 5$$

Where:

$f_r = Reduced\ Frequency\ at\ the\ Reference\ Temperature\ (Hz)$

$f = Actual\ Test\ Frequency\ at\ the\ Test\ Temperature\ (Hz)$

The AASHTO Mechanistic Empirical Pavement Design Guide (MEPDG) uses the following sigmoidal model to estimate the dynamic modulus of an asphalt mix for curve fitting purposes:

$$\log|E^*| = \delta + \frac{\alpha}{1 + e^{\beta + \gamma(\log f_r)}} \qquad Eq. 6$$

Where

$|E^*| = Dynamic\ Modulus\ (10^6\ psi)$

$\delta, \alpha, \beta, \gamma = Fitting\ Parameters$

$\delta = \ the\ minimum\ value\ of\ E^*\ (10^6\ psi)$

$\delta + \alpha = \ the\ maximum\ value\ of\ E^*\ (10^6\ psi)$

$\beta\ and\ \gamma = \ the\ shape\ of\ the\ sigmoidal\ function\ and\ are\ dimensionless$

By using the Solver feature in Microsoft Excel, the laboratory calculated dynamic modulus can be compared to the dynamic modulus estimated using the sigmoidal equation and minimizing the sum of the square of the Error, defined as follows:

$$Error^2 = \left[\frac{E^*_{Lab} - E^*_{Sigmoidal}}{E^*_{Lab}}\right]^2 \qquad Eq.7$$

The error is calculated for each frequency and temperature and then summed for the entire data set (Σ Error^2). In Solver, the objective cell is the (Σ Error^2), it is set to become as low as possible (min.) by changing δ, α, β, γ, C_1, C_2, and C_3 using an iteration method. The following table is a summary of the curve fitting parameters and regression coefficients solved in Solver for each layer.

Table 4.12 Curve Fitting Parameters and Regression Coefficients

Site	Layer	δ	α	β	γ	c_1	c_2	c_3
HiMA	Surface	0.485	-2.250	0.859	0.421	6.712	-0.120	0.00034
	Intermediate	0.495	-2.341	1.049	0.452	5.451	-0.089	0.00016
	AC Base (Kraton)	0.631	-2.431	1.131	0.411	5.700	-0.093	0.00017
	AC Base (Control)	0.605	-2.648	1.269	0.438	5.315	-0.083	0.00011

The results of the dynamic modulus master curves as a function of reduced frequency and shift factors as a function of temperature for the 442 surface mix, 442 Intermediate mix, 302 AC Base mix (with Kraton binder), and the 302 AC Base mix (control binder) for the HiMA study in the APLF are shown in the following figures:

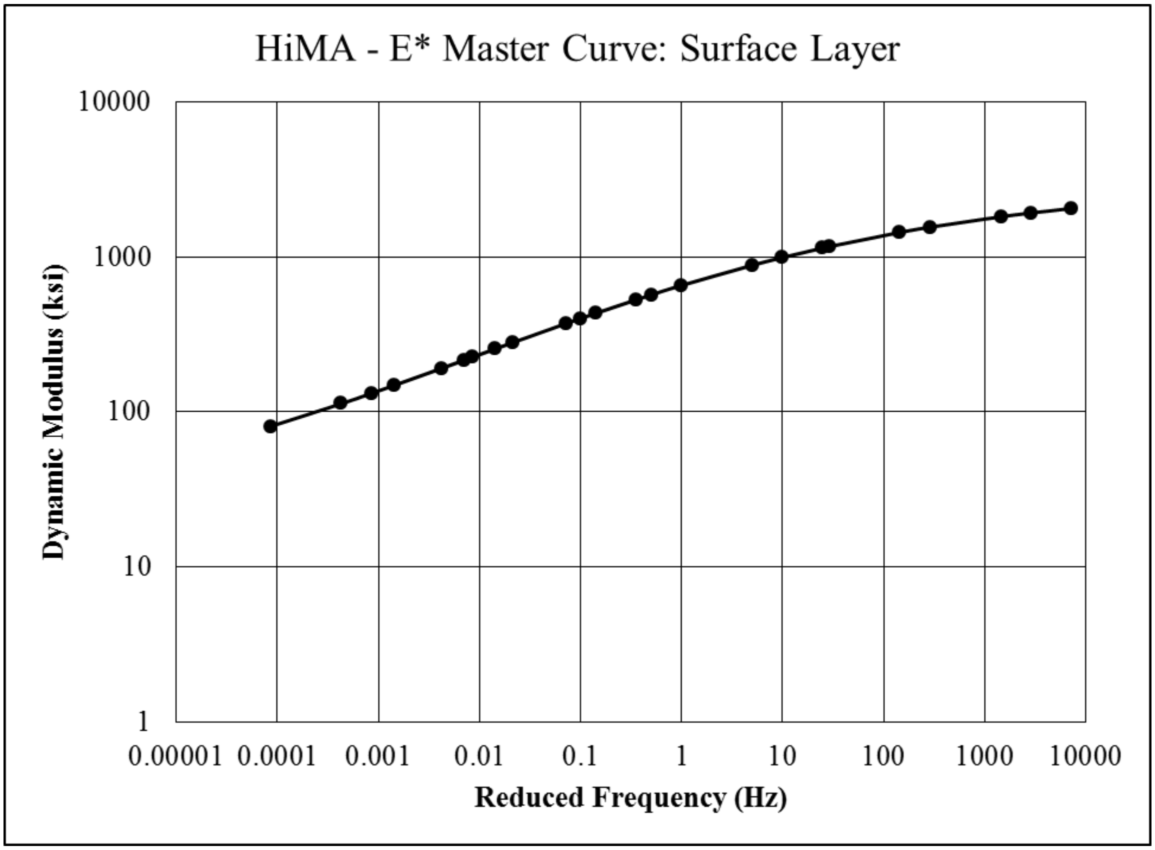

Figure 4.8 Dynamic Modulus Master Curve for 442 Surface Layer-HiMA

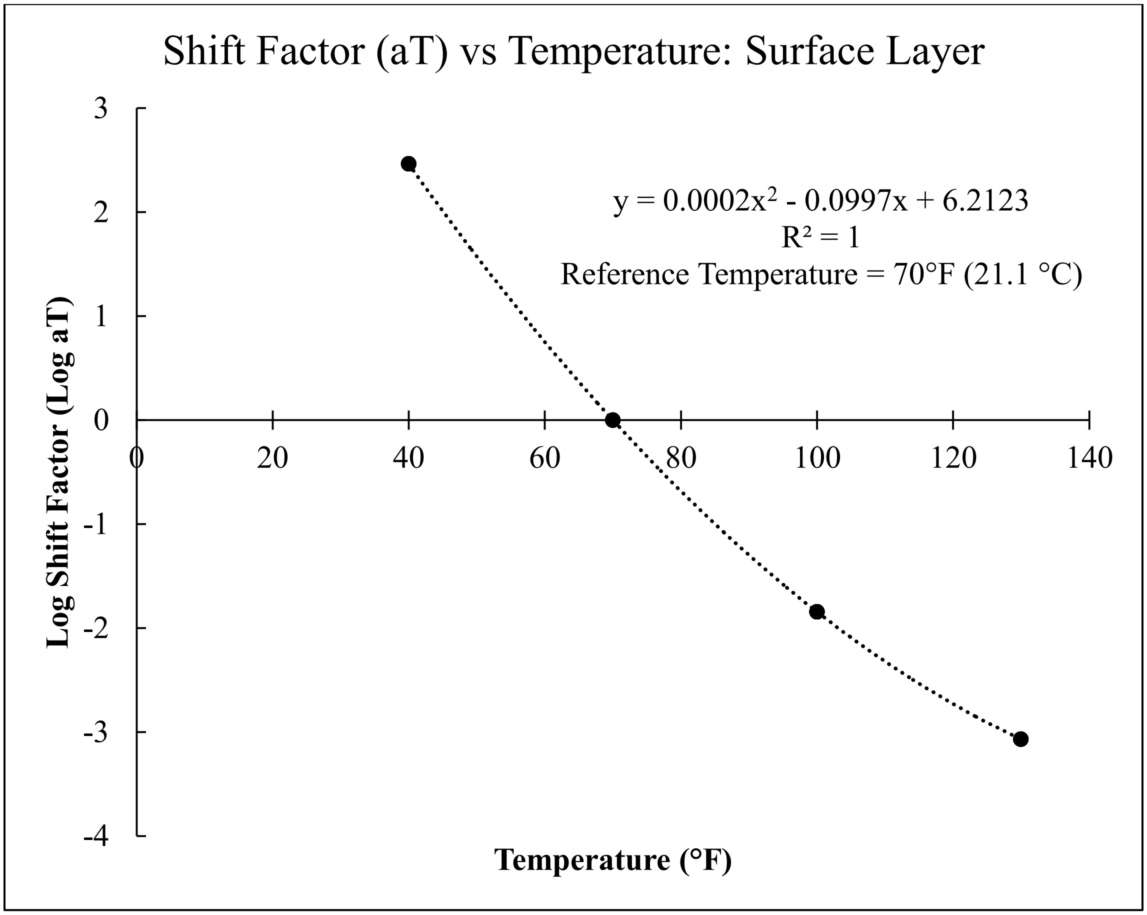

Figure 4.9 Shift Factor vs. Temperature for 442 Surface Layer-HiMA

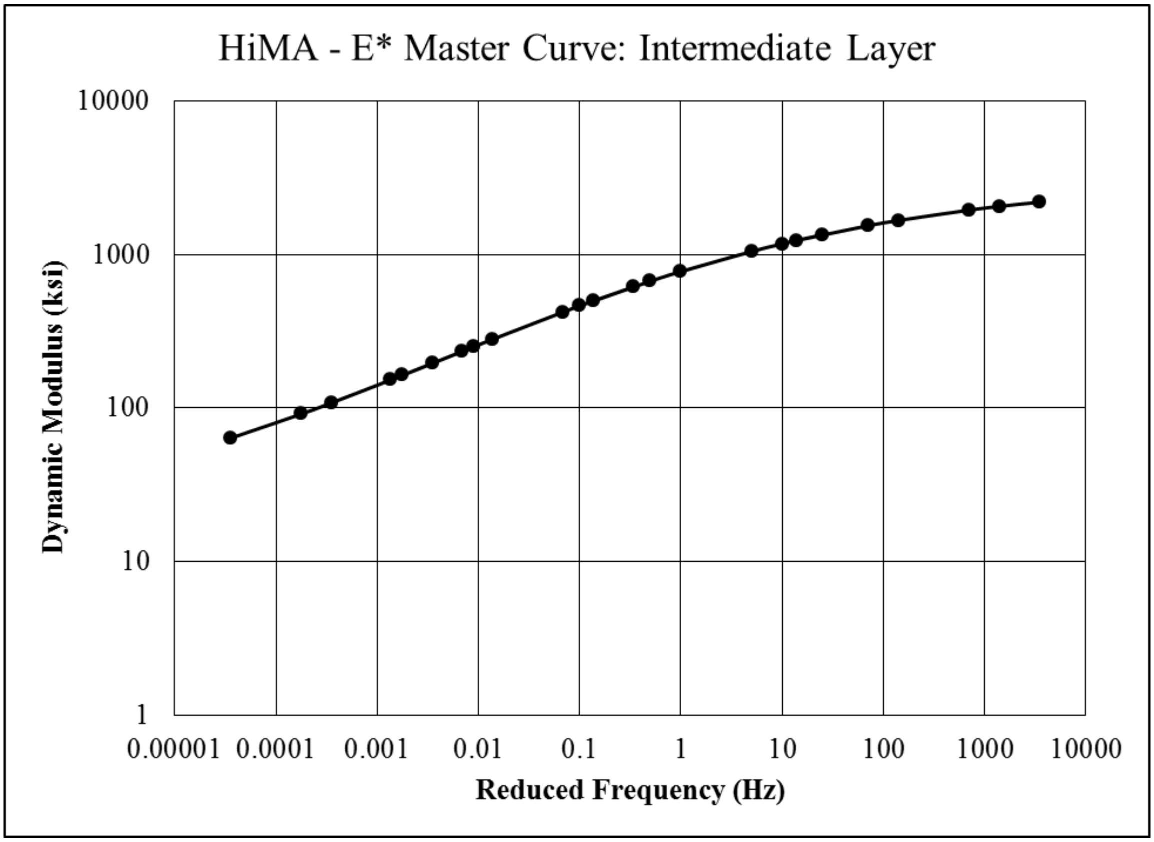

Figure 4.10 Dynamic Modulus Master Curve for 442 Intermediate Layer-HiMA

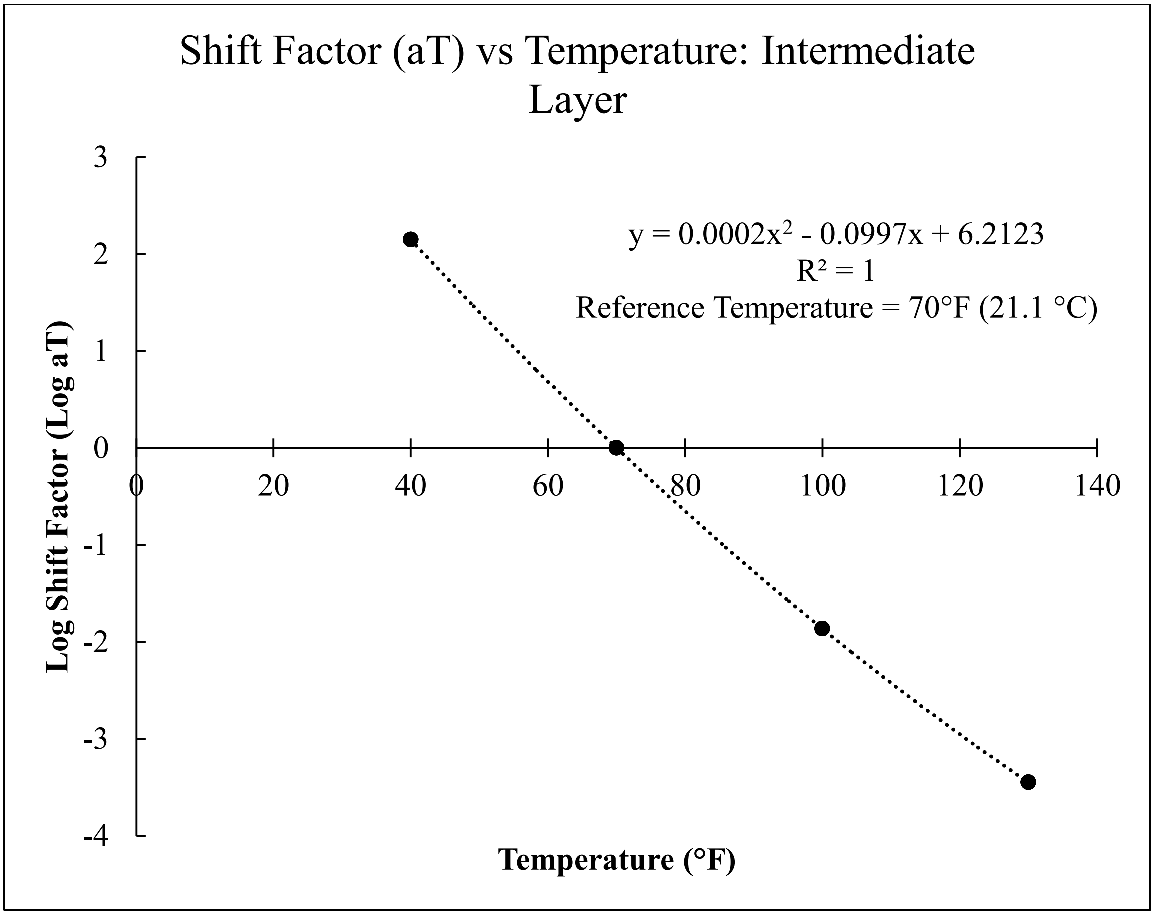

Figure 4.11 Shift Factor vs. Temperature for 442 Intermediate Layer-HiMA

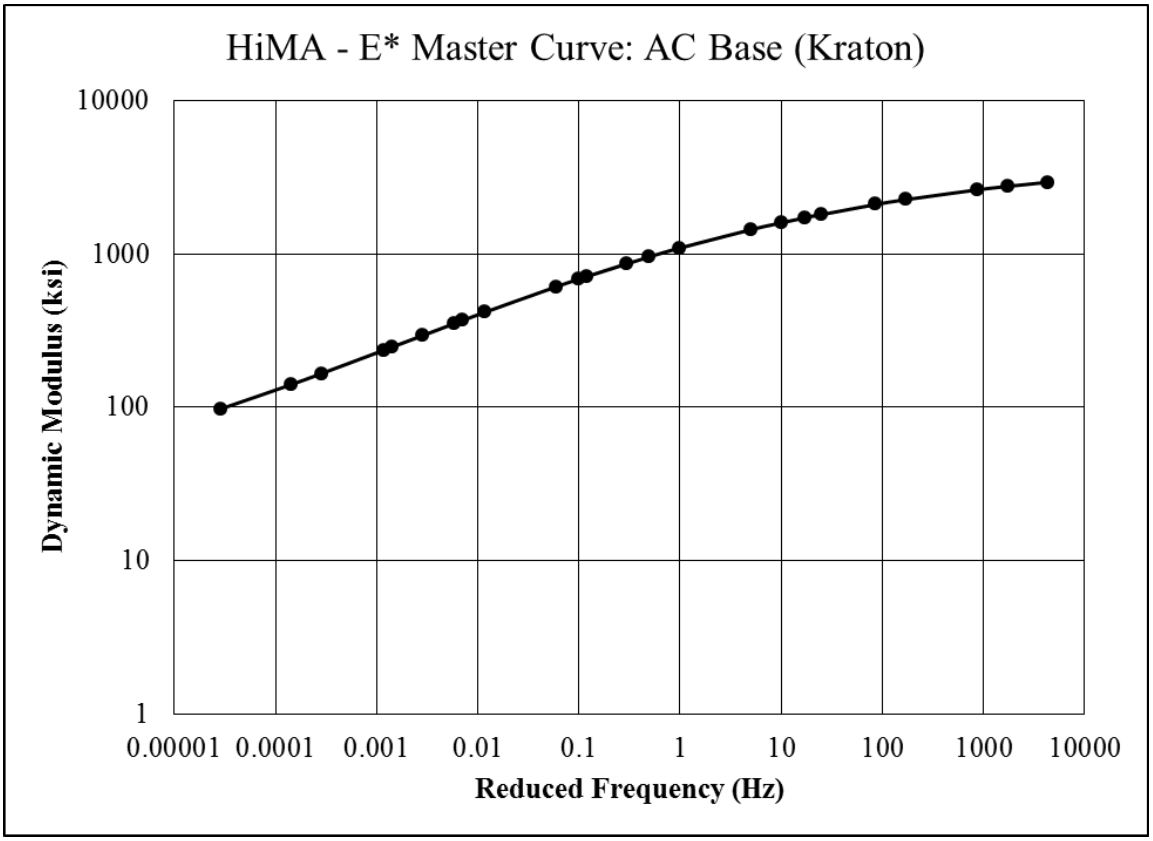

Figure 4.12 Dynamic Modulus Master Curve for 302 AC Base (with Kraton Binder)-HiMA

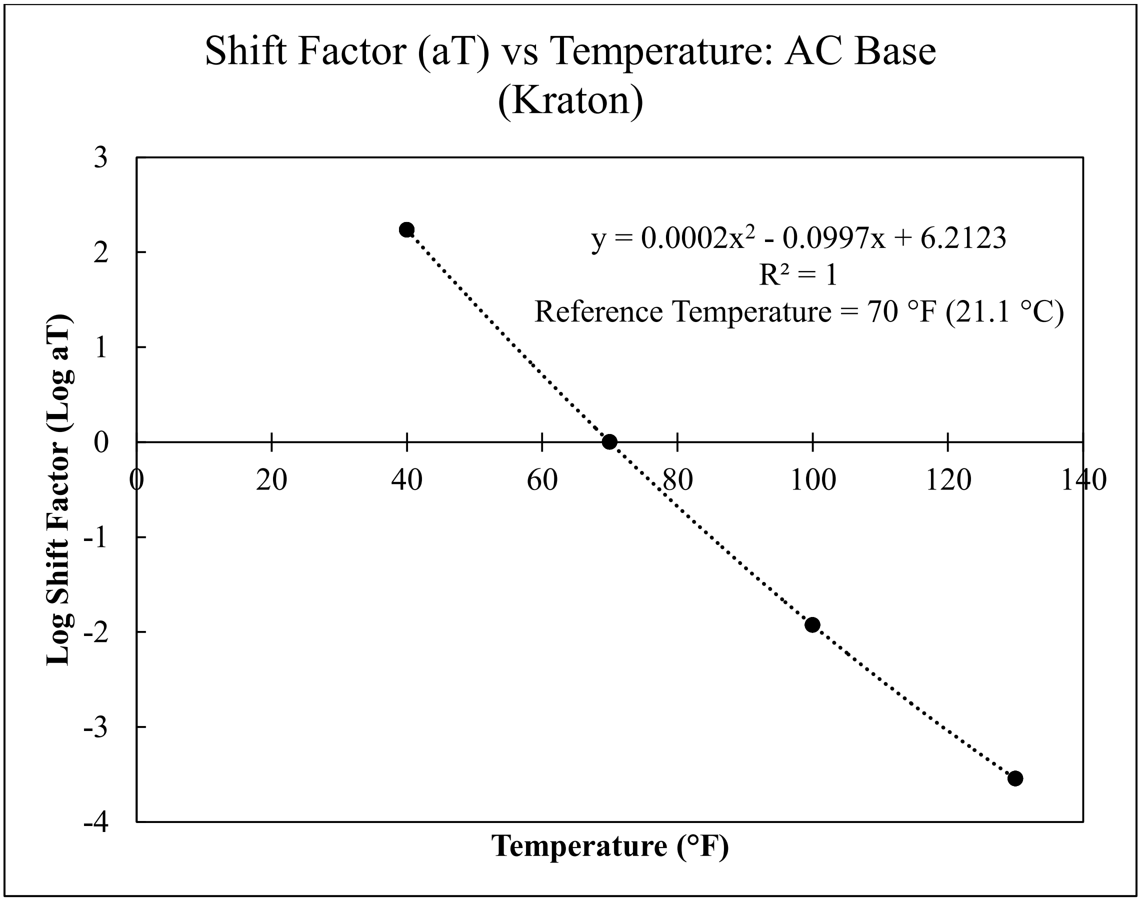

Figure 4.13 Shift Factor vs. Temperature for 302 AC Base (with Kraton Binder)-HiMA

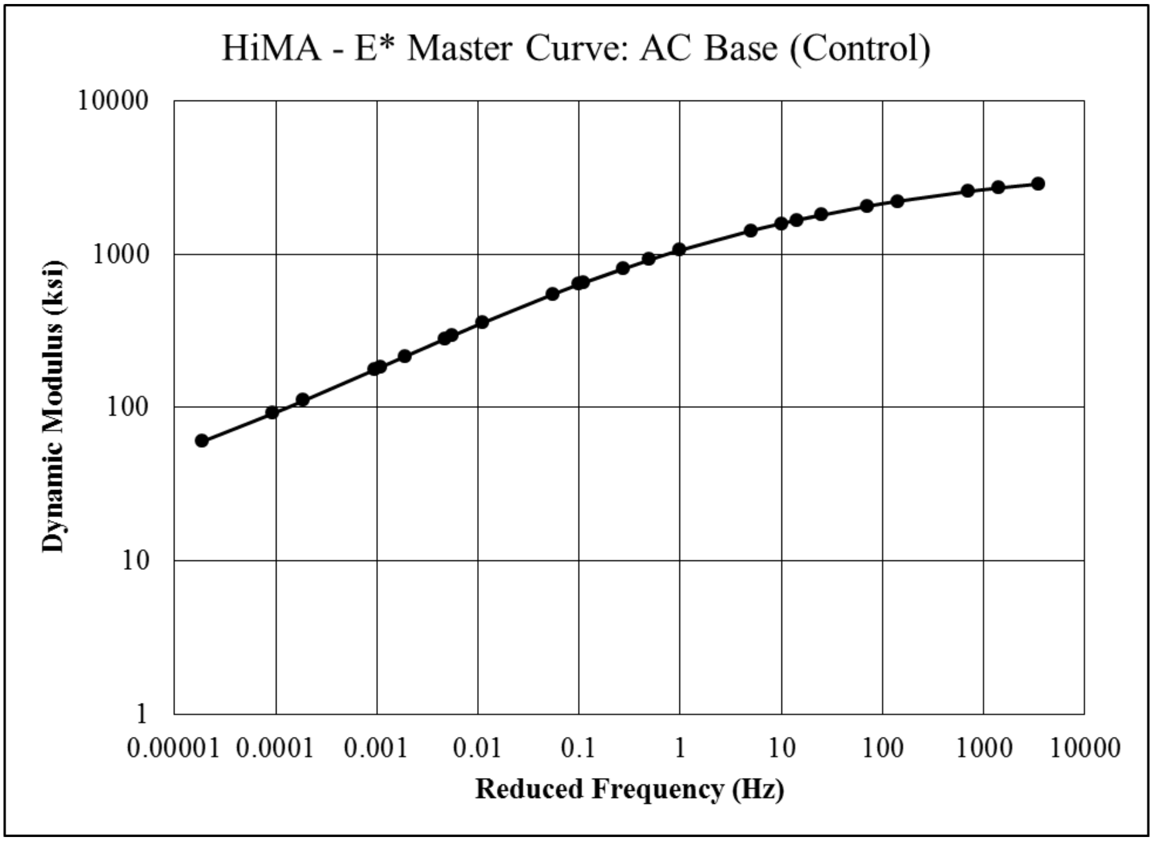

Figure 4.14 Dynamic Modulus Master Curve for 302 AC Base (with Control Binder)-HiMA

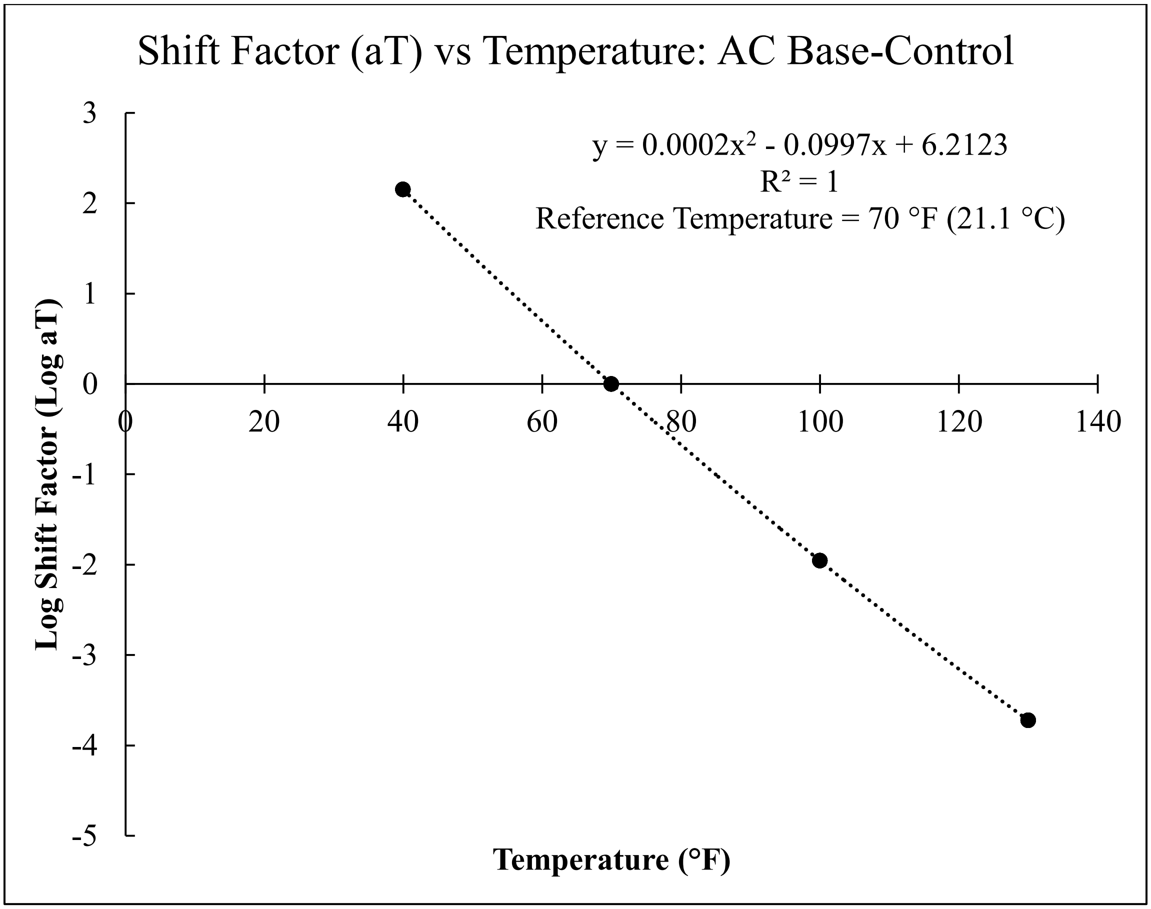

Figure 4.15 Shift Factor vs. Temperature for 302 AC Base (with Control Binder)-HiMA

4.8 Endurance Limits Based on Laboratory Tested Temperatures

Table 4.13 is a summary of the endurance limits for the AC base mixes used in the APLF when using the NCHRP assumption that the dynamic modulus is equal to the initial flexural stiffness ($E_0 = E^*$):

Table 4.13 Estimation of Endurance Limit when E_0 = E*, RP = 5 seconds, f = 10 Hz, N = 200000, SR = 1.

Site	Mix	Test Temp *T*		Dynamic Modulus *E**		Initial Flexural Stiffness E_0		Endurance Limit ε_t
		(°F)	(°C)	(ksi)	(GPa)	(ksi)	(GPa)	(με)
HiMA APLF	AC Base: Control	40	4.4	2729	18.82	2729	18.82	68
		70	21.1	1515	10.45	1515	10.45	80
		100	37.8	677	4.67	677	4.67	99
	AC Base: Kraton	40	4.4	2622	18.08	2622	18.08	69
		70	21.1	1591	10.97	1591	10.97	79
		100	37.8	653	4.5	653	4.5	100

Table 4.14 is a summary of the endurance limits for the AC base mixes used in the APLF when using the Kansas assumption that the dynamic modulus is equal to twice the value of the initial flexural stiffness ($E_0 = E^*/2$).

Table 4.14 Estimation of Endurance Limit when E_0 = E*/2, RP = 5 seconds, f = 10 Hz, N = 200000, SR = 1.

Site	Mix	Test Temp *T*		Dynamic Modulus *E**		Initial Flexural Stiffness E_0		Endurance Limit ε_t
		(°F)	(°C)	(ksi)	(GPa)	(ksi)	(GPa)	(με)
HiMA APLF	AC Base: Control	40	4.4	2729	18.82	1365	9.41	82
		70	21.1	1515	10.45	757	5.22	96
		100	37.8	677	4.67	339	2.34	118
	AC Base: Kraton	40	4.4	2622	18.08	1311	9.04	83
		70	21.1	1591	10.97	795	5.48	95
		100	37.8	653	4.5	326	2.25	119

As shown in Table 4.13 and Table 4.14, larger FEL were found using the Kansas assumption ($E_0 = E^*/2$) when comparing the two methods for estimating the fatigue endurance limits. Additionally, the FEL were found to be the highest when the pavement temperatures were the hottest.

4.9 Comparison of Endurance Limits and Strain Results from APLF Testing

Since temperatures used during laboratory testing are not always equal to temperatures measured in the field, relationships between the two must be developed to better estimate the endurance limits of the pavement structures. These relationships are based on a second-order polynomial regression curve for each mix that is based on the dynamic modulus at 10 Hz versus test temperature. The following equation was used to describe this relationship:

$$E^*(T) = aT^2 + bT + c \qquad Eq. 2$$

Where:

T = Test Temperature (°F)

a, b, c = Regression Coefficients

Table 4.15 represents a summary of the dynamic modulus testing versus temperature at a frequency of 10 Hz and Table 4.16 represents a summary of the resulting regression coefficients.

Table 4.15 Dynamic Modulus Results at 10 Hz

Temperature		Dynamic Modulus at 10 Hz			
		HiMA-AC Base-Kraton		APLF-AC Base-Control	
(°F)	(°C)	(ksi)	(GPa)	(ksi)	(GPa)
40	4.4	2769	19.09	2729	18.82
70	21.1	1552	10.70	1515	10.45
100	37.8	733	5.05	677	4.67
130	54.4	290	2.00	211	1.45

Table 4.16 Second Order Regression Coefficients for Each Mix

AC Base Mix	Regression Coefficients			
	a (ksi/°F^2)	*b* (ksi/°F)	*c* (ksi)	R^2
HiMA-AC Base-Kraton	0.2147	-64.015	4984	0.9996
HiMA-AC Base-Control	0.2077	-63.286	4927.9	0.9971
	a_c (GPa/°C^2)	b_c (GPa/°C)	c_c (GPa)	R^2
HiMA-AC Base-Kraton	0.0048	-0.6239	21.7555	0.9996
HiMA-AC Base-Control	0.00464	-0.6204	21.4802	0.9971

As mentioned in Chapter 2, one way to determine if a pavement structure meets the perpetual concept is to use the model created by Witczak et al. (2013). In this model if the stiffness ratio is greater than or equal to 1.0 the pavement is said to be perpetual. Therefore, using average maximum longitudinal strains determined during field testing in the APLF and inserting these strains into the model designed by Witczak et al. while solving for the stiffness ratio, each test section could be categorized as meeting or not meeting the perpetual qualification. In addition, the dynamic modulus used was based on the temperature measured in the APLF, and using the second-order polynomial equations for each mix will ensure the modulus used in each section will accurately estimate conditions in the AC base layers. Table 4.17 and Table 4.18 show the FEL of the HiMA test temperatures and the results of the stiffness ratio when the average maximum longitudinal strains measured are substituted into the model created by Witczak et al.

Table 4.17 Fatigue Endurance Limits at Test Temperatures (E_0 = E*), RP = 5 seconds, f = 10 Hz, N = 200000, SR = 1

Mix	Test Temp *T*		Dynamic Modulus *E**		Initial Flexural Stiffness E_0		FEL ε_t
	(°F)	(°C)	(ksi)	(GPa)	(ksi)	(GPa)	(με)
AC Base: Control	70	21	1515	10.45	1515	10.45	80
	100	38	677	4.67	677	4.67	99
AC Base: Kraton	70	21	1552	10.7	1552	10.7	79
	100	38	733	5.05	733	5.05	97

Table 4.18 Stiffness Ratio Based on the Average Peak Strain Measured during the Controlled Load Tests ($E_0 = E^*$), RP = 5 seconds, f = 10 Hz, N = 200000

Lane	Mix	Pavement Thickness	Test Temp T	Dynamic Modulus E^*	Initial Flexural Stiffness E_0	Stiffness Ratio SR	Avg. Peak Strain	FEL ε_t
		(in)	(°F)	(ksi)	(ksi)		(με)	(με)
D	AC Base: Control	11	70	1515	1515	1.10	52	80
			100	677	677	1.14	56	99
C	AC Base: Kraton	10	70	1552	1552	1.13	46	79
			100	733	733	1.11	61	97
B	AC Base: Kraton	9	70	1552	1552	1.06	62	79
			100	733	733	1.05	79	97
A	AC Base: Kraton	8	70	1552	1552	1.03	70	79
			100	733	733	**0.98**	106	97

Based on the results of the HiMA testing using the NCHRP assumption ($E_0 = E^*$), Lane A did not meet the criteria for perpetual pavements by having a stiffness ratio of 0.98. Table 4.19 and Table 4.20 show the results of the endurance limit using the Kansas assumption when the initial flexural stiffness is half of the dynamic modulus.

Table 4.19 Fatigue Endurance Limit at Test Temperatures ($E_0 = E^*/2$), RP = 5 seconds, f = 10 Hz, N = 200000, SR = 1

Mix	Test Temp T		Dynamic Modulus E^*		Initial Flexural Stiffness E_0		FEL ε_t
	(°F)	(°C)	(ksi)	(GPa)	(ksi)	(GPa)	(με)
AC Base: Control	70	21	1515	10.45	757	5.22	96
	100	38	677	4.67	339	2.34	118
AC Base: Kraton	70	21	1552	10.7	776	5.35	95
	100	38	733	5.05	367	2.53	116

Table 4.20 Stiffness Ratio Based on the Average Peak Strain Measured during the Controlled Load Tests (E0 = E*/2), RP = 5 seconds, f = 10 Hz, N = 200000

Lane	Mix	Pavement Thickness	Test Temp T	Dynamic Modulus E^*	Initial Flexural Stiffness E_0	Stiffness Ratio SR	Avg. Peak Strain	FEL ε_t
		(in)	(°F)	(ksi)	(ksi)		(με)	(με)
D	AC Base: Control	11	70	1515	757	1.15	52	96
			100	677	339	1.19	56	118
C	AC Base: Kraton	10	70	1552	776	1.18	46	95
			100	733	367	1.16	61	116
B	AC Base: Kraton	9	70	1552	776	1.11	62	95
			100	733	367	1.10	79	116
A	AC Base: Kraton	8	70	1552	776	1.03	70	95
			100	733	367	1.02	106	116

Based on the results of the HiMA testing using the Kansas assumption ($E_0 = E^*/2$), Lane A met the criteria for perpetual pavements unlike the previous analysis using the NCHRP assumption ($E_0 = E^*$). In addition, when using the Kansas assumption all of the lanes in the APLF are considered perpetual based on the model created by Witczak et al., (2013).

4.10 Rutting Evaluation

The asphalt mixes tested in the APLF appeared to be very resistant to rutting. The 8 inch test section exhibited the highest peak strains for both temperatures. This section was analyzed as an example to show the minimal amounts of rutting measured in the test pavements. Rutting was measured to be 0.012 in. (0.303 mm) in the 8 inch test section (Lane A) after 10,000 wheel passes conducted at 70°F (21.1°C). Additionally, the accumulated rutting was measured after 10,000 wheel passes conducted at 100°F (37.8°C) and was found to be 0.046 in. (1.168 mm). The following figure shows the profile history at 70°F (21.1°C) in the 8 inch after profiles were taken after wheel passes of 100, 300, 1000, 3000, and 10,000 with the wheel loaded to 9,000 lbs, whereas Figure 4.17 shows the profile history with testing conducted at 100°F (37.8°C). Both figures show the initial profiles of the 8 inch section as a bolded line and indicated by the number "0" and the 10,000 passes indicated by the dotted lined.

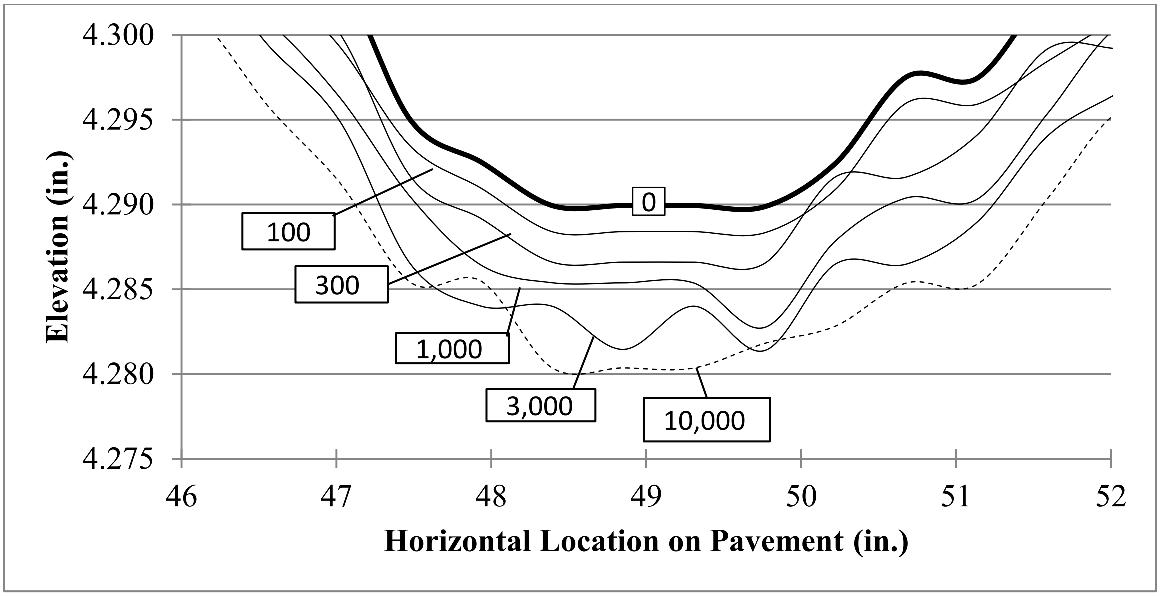

Figure 4.16 Profile History in 8 Inch Section (Lane A) at 70℉ (21.1℃)

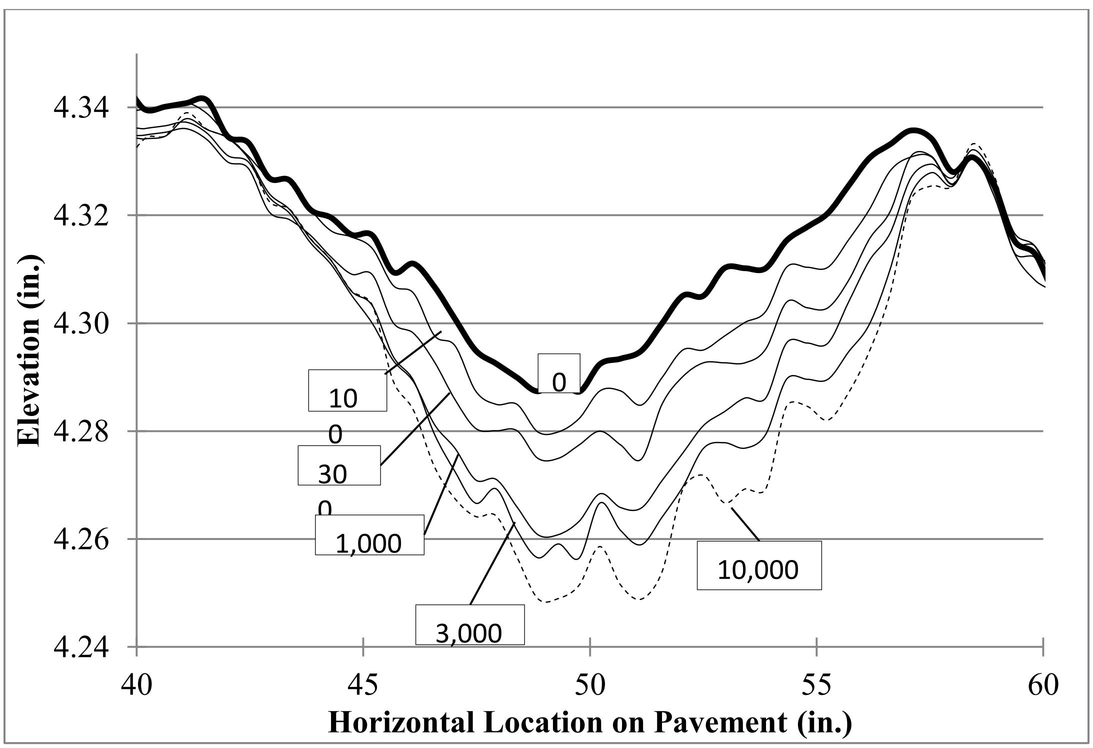

Figure 4.17 Profile History in 8 Inch Section (Lane A) at 100℉ (37.8℃)

Further evaluation was performed at locations that showed the largest rutting in each test section. Maximum rutting values were calculated by subtracting the original profile elevation by each successive profile section elevations. The maximum difference in elevations in each test section occurred along the wheel path while the APLF test sections were kept at a temperature of 100°F (37.8°C). The following table shows the rutting results of the HiMA test sections.

Table 4.21 Maximum Depth of rutting for APLF Lanes at 100°F (37.8°C)

Number of Passes	**Lane A**		**Lane B**		**Lane C**		**Lane D**	
	(in)	**(cm)**	**(in)**	**(cm)**	**(in)**	**(cm)**	**(in)**	**(cm)**
100	0.013	0.032	0.009	0.023	0.013	0.034	0.012	0.030
300	0.020	0.051	0.016	0.041	0.022	0.055	0.025	0.065
1,000	0.029	0.074	0.026	0.066	0.037	0.093	0.038	0.096
3,000	0.036	0.091	0.036	0.091	0.038	0.095	0.054	0.137
10,000	0.046	0.117	0.050	0.128	0.054	0.138	0.069	0.174
Pavement thickness	8	20	9	23	10	25	11	28

The maximum values from the previous table were plotted against the number of passes at 9000 lb (40 kN) load and can be seen in the following figure.

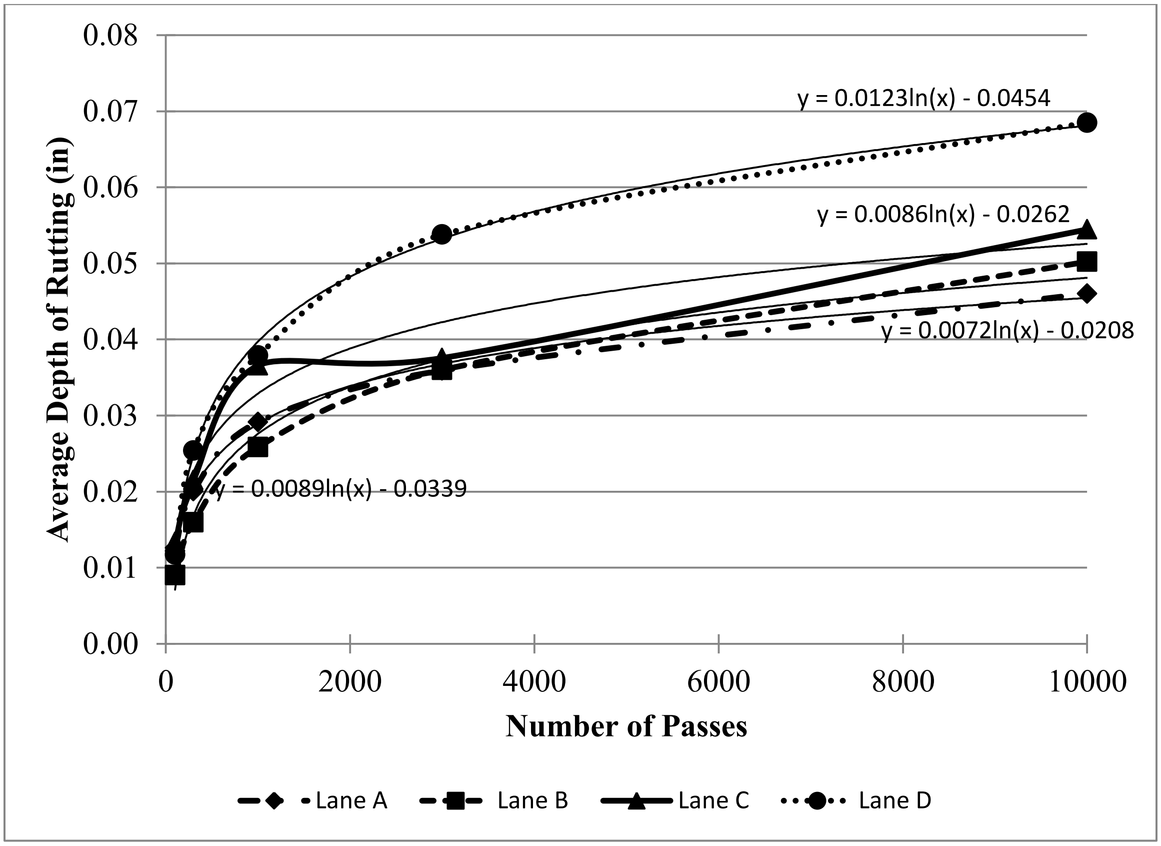

Figure 4.18 Depth of Rutting vs. Number of Passes for HiMA

Using the trendlines produced in the previous figure, logarithmic equations were used to model the rutting behavior of each test section for the HiMA study. The following table shows the trendline parameters that are based on the following equation:

$y = A*\ln x + B$.

Table 4.22 Trendline Parameters for HiMA Lanes

Pavement Section	**Trendline Parameters at 100°F (37.8°C)**			
	A (in.)	**A (cm.)**	**B**	**R^2**
Lane A	0.0072	0.0183	-0.0208	0.9982
Lane B	0.0089	0.0226	-0.0339	0.9868
Lane C	0.0086	0.0218	-0.0262	0.9598
Lane D	0.0123	0.0312	-0.0454	0.9979

ODOT has four classifications for rutting: high, medium, low, and none. High rutting consists of any rut depth that exceeds 0.75 in. (1.91 cm), medium rutting falls between 0.75 in. – 0.375 in. (1.91 cm – 0.95 cm), low falls between 0.375 in. – 0.125 in (0.95 cm – 0.32 cm), and any rutting below 0.125 in. (0.32 cm) is considered "No Rutting" (Sargand et al., 2009). For this project no rut values were found to exceed the "Low Rut" threshold of 0.125 in (0.32 cm), as shown in Table 4.22.

Since only one type of surface mix was used in the HiMA project, rutting data from the WMA project in 2009 had to be used to compare against the HiMA surface mix. Table 4.23 and Table 4.24 show the volumetric properties and the maximum rutting depths found in the HiMA and WMA projects while the test sections were maintained at 100°F (37.8°C). The Aspha-min and Control surface mixes were chosen to compare against the HiMA surface mix.

Table 4.23 Volumetric Properties for WMA Surface Mixes and HiMA Surface Mix

Layer	Surface-Control	Aspha-min WMA	HiMA Surface
Mix	446	446	442
Gradation			
2" (50.8 mm)	100	100	100
1 1/2" (38 mm)	100	100	100
1" (25.4 mm)	100	100	100
3/4" (19 mm)	100	100	100
1/2" (12.5 mm)	100	100	100
3/8" (9.5 mm)	92	92	93
#4 (4.75 mm)	51	51	57
#8 (2.36 mm)	38	38	38
#16 (1.18 mm)	28	28	27
#30 (0.600 mm)	18	18	19
#50 (0.300 mm)	7	7	11
#100 (0.150 mm)	4	4	7
#200 (0.075 mm)	2.8	2.5	4.8
Agg. Blend G_{sb}	2.612	2.612	2.393
G_{mm}	2.429	2.429	2.440
% Binder Content	6.1	6.1	5.7
% Virgin Binder	5.3	5.3	5.0
Asphalt Binder	PG 70-22	PG 70-22	PG 88-22
Design, Air Voids (%)	3.5	3.5	3.5
F/A	0.5	0.5	0.8
RAP %	15	15	15

Table 4.24 Maximum Depth of Rutting for APLF and WMA Surface Mixes

Number of Passes	HiMA (2014)		WMA 3N (2009) Aspha-min		WMA 4N (2009) Control	
	(in)	**(cm)**	**(in)**	**(cm)**	**(in)**	**(cm)**
100	0.012	0.030	0.046	0.116	0.025	0.064
300	0.025	0.065	0.065	0.165	0.040	0.102
1,000	0.038	0.096	0.096	0.244	0.066	0.169
3,000	0.054	0.137	0.137	0.348	0.105	0.267
10,000	0.069	0.174	0.202	0.513	0.174	0.441

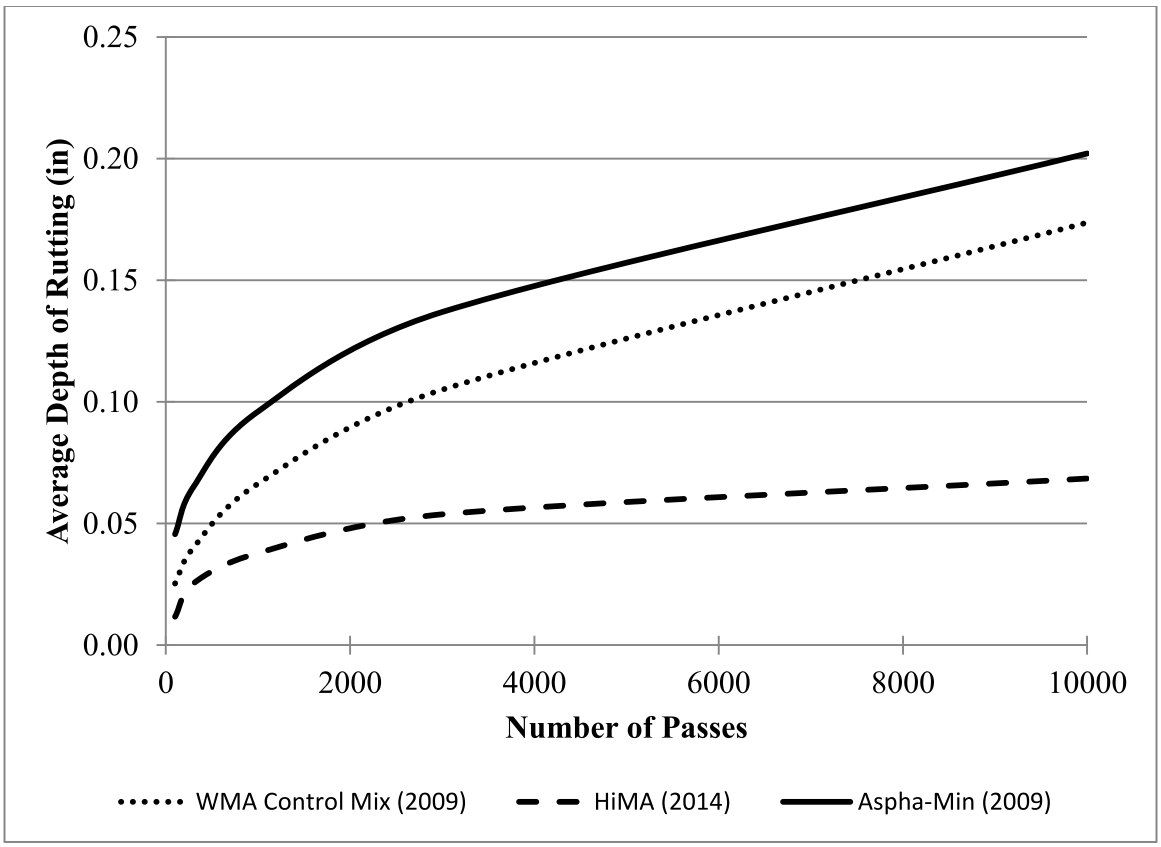

Figure 4.19 Comparison of Rut Depths between HiMA and WMA Mixes

As shown in the previous figure, the HiMA produced much lower rutting over the same amount of loading passes. To determine how much more rut resistant the HiMA was compared to the WMA mixes, further numerical analysis was completed. Using the ODOT classification for “Low Rut” and arranging the trendline parameter equation discussed previously for the HiMA and the trendline parameter equation from the WMA report, the number of passes could be solved for by setting the rut depth equal to 0.125 in. (0.32 cm) and solving for the number passes. The following table shows the results to using this technique.

Table 4.25 Number of passes to Reach Low Rutting Classification

Mix	**Number of Passes to Reach Low Rutting Classification**
HiMA	1038885
Aspha-Min	2260
Control	4551

The previous table shows that the HiMA would need over 1 million passes at 9000 lbs (40 kN) to reach low rutting. This value is significantly more than the Aspha-Min (2260 Passes) and the Control (4551 Passes).

In 2013, NCAT created Report 13-03, in this report, NCAT compared a 5.75 in. (14.6 cm) HiMA Kraton mix section to a control section that consisted of 7 in. (17.8 cm) of AC. Results found in the NCAT report stated that there was a significantly lower rate of rutting found in the HiMA compared to the control AC (Timm et al., 2013). Based off the findings between the APLF and the WMA projects, this report agrees with that claim.

The rutting results of the HiMA study supports that the HiMA binder is very beneficial in resisting rutting in the surface and intermediate layers.

CHAPTER 5: CONCLUSIONS AND RECOMMENDATIONS

The main objective of this study was to develop an optimal design thickness for perpetual pavements in Ohio. Other secondary objectives of this project included:

- Monitoring four pavement structures containing highly modified asphalt (HiMA) with varied thickness of AC base layers.
- Evaluate the effect of an increase in temperature on the rutting and strains within each HiMA test section pavement.
- Evaluate the effect of wheel position over pavements with respect to strains in each layer of the pavements.
- Conduct laboratory testing on the various pavement mixes used within the APLF and determine mix specific fatigue endurance limits.

5.1 Conclusions

Following the field and laboratory testing conducted at the Accelerated Pavement Loading Facility on varying depths of highly modified polymer asphalt mixes the following conclusions were made:

- The use of highly modified polymer binder within the AC Base layers of the tested sections proved to provide a high resistance to rutting; however, the modified binder did not show additional structural support within the test pavement base layers between the modified and unmodified sections during the time of testing.
- Under the two assumptions analyzed during this project to estimate the fatigue endurance NCHRP ($E_0 = E^*$) and Kansas ($E_0 = E^*/2$), the conservative NCHRP

assumption determined all the test sections besides the thinnest 8 inch test section yielded strains below their estimated thresholds; whereas, the Kansas assumption determined all the sections yielded strains below their estimated thresholds.

- When analyzing longitudinal strains in the bottom of the AC base layers, the thinnest 8 inch section with the highly modified binder produced the largest magnitude of strains under both temperatures of 70°F (21.1°C) and 100°F (37.8°C), while the lowest magnitude of strains was found in the modified 10 inch section and the control 11 inch section. The modified 10 inch section yielded lower strain values than all the other sections at 70°F (21.1°C), while the 11 inch control section yielded lower strain values when the test sections were maintained at 100°F (37.8°C).
- Using the LVDT and surface rutting data gathered throughout dynamic wheel loading testing conducted within the APLF; this report agrees with the findings NCAT 13-03 report. In this report, suggestions of implementing HiMA pavements were made to be used to significantly reduce surface rutting.
- When analyzing the effect of wheel wondering, it was determined that the highest magnitude of strains were generated when the tandem wheel was offset 6 inches from the centerline. This phenomenon was experienced under all three loading conditions at both temperatures in every test pavement within the APLF.
- Transverse strains measured in the bottom of the AC Base were found to be less than the longitudinal strains at the same location. A relationship was found between the transverse and longitudinal strains while the test pavements were

maintained at 70°F (21.1°C). This relationship could not be explored at the 100°F (37.8°C) due to the test pavement's intermediate layer never switching from compressive to tensile strains as dynamic wheel loading was being applied to each test section.

5.2 Recommendations

Once dynamic testing was completed in the Accelerated Pavement Loading Facility on varying depths of highly modified polymer asphalt mixes the following recommendations could be made:

- Further testing should be completed on the use of highly modified asphalt pavements before an optimal thickness can be definitively chosen to be implemented in Ohio. Although, upon completion of testing conducted in the APLF, a recommendation may be made that using a similar design and mix as the 9 inch HiMA section built upon a 6 inch DGAB and constructed on a chemically stabilized subgrade would be sufficient to create a perpetual pavement at temperatures of 70°F (21.1°C) and 100°F (37.8°C).
- Based on the information found from the literature review, cold weather testing (40°F and below) should be conducted on the highly modified asphalt pavements within the APLF. Since colder conditions have been found to decrease the FEL of asphalt pavements, cold weather testing needs to be completed to ensure the pavements in the APLF remain below the FEL thresholds.

- Further research should be conducted to investigate the relationship between the initial modulus E_0 as measured during the beam fatigue test and E^* measured during the asphalt mixture performance test.
- An economic analysis should be performed to determine the cost effectiveness of using the highly modified asphalt mixes compared to standard hot mix asphalt mixes.
- With only 20,000 total passes being completed per test section in the APLF, higher amounts of passes should be completed to determine how aging effects the pavements as well as confirming the rutting resistance of the highly modified asphalt.
- HiMA pavements should be tested out in field conditions to determine the effects of weathering as well as other destructive damages that may occur with in-situ pavements.

REFERENCES

Adlinge, S. S., & Gupta, A. K. (2013). Pavement Deterioration and its Causes. *International Journal of Innovative Research and Development*, *2*(4), 437-450.

Asphalt Pavement Alliance (APA). 2002. *Perpetual Pavements: A Synthesis*. APA 101, Lanham, Maryland.

Asphalt Pavement Alliance. (2010). *Asphalt pavement: America rides on US*. (IM-41). Lanham, MD.

Carpenter, S. H., Ghuzlan, K. A., & Shen, S. (2003). Fatigue endurance limit for highway and airport pavements. *Transportation Research Record: Journal of the Transportation Research Board*, *1832*(1), 131-138.

El-Hakim, M.Y., S.L. Tighe, & K.A. Galal. 2009. M-E Performance Evaluation and LCCA of a Conventional Asphalt Pavement and a Perpetual Asphalt Pavement Section. *Proceedings. International Conference on Perpetual Pavements. Ohio University .Columbus, Ohio.*

Federal Highway Administration. (2013). *2013 Status of the Nation's Highways, Bridges, and Transit: Conditions & Performance*. Report to Congress. (Chapter 6: Finance).

Heitzman, M. & Coree, B. (2004). A case study of three full-depth HMA interstate pavements. *International Symposium on Design and Construction of Long Lasting Asphalt Pavements*, pp. 843–858, 2004 (International Society for Asphalt Pavements: Auburn, Alabama).

Jordan, B. Benjamin., & Sargand, M. Shad. (2014). Asphalt Perpetual Pavement Design: Utilizing Existing Pavement Systems in Ohio. *Proceedings. International Conference on Perpetual Pavements. Ohio University .Columbus, Ohio.*

Kluttz, R. Q., Molenaar, A. A. A., van de Ven, M. F. C., Poot, M. R., Liu, X., Scarpas, A., & Scholten, E. J. (2009). Modified Base Courses for Reduced Pavement Thickness and Improved Longevity. *In Proceedings of the International Conference on Perpetual Pavement.*

Little, D. N., & Nair, S. (2009). Recommended practice for stabilization of subgrade soils and base materials. *National Cooperative Highway Research Program, Transportation Research Board of the National Academies.*

Molenaar, A. A., van de Ven, M. F., Poot, M., Li, N., & SCHOLTEN, E. J. (2011, September). SBS Polymer Modified Base Course Mixtures for Heavy Duty Pavements. In *AAPA International Flexible Pavements Conference, 14th, 2011, Sydney, New South Wales, Australia*.

Monismith, C.L., & McLean, D. B. (1972). *Structural Design Considerations.* Proceedings of the Association of Asphalt Paving Technologists, 1972 (Vol.41).

Moreno, F., & Rubio, M. C. (2013). Effect of aggregate nature on the fatigue-cracking behavior of asphalt mixes. *Materials & Design*, *47*, 61-67.

Newcomb, D. E., Buncher, M., & Huddleston, I. J. (2001). Concepts of perpetual pavements. *Transportation Research Circular*, *503*, 4-11.

Newcomb, D. E., & Hansen, K. R. (2006). Mix type selection for perpetual pavements. In *Proceedings*.

Newcomb, D. E., Willis, R., & Timm, D. H. (2010). *Perpetual asphalt pavements a synthesis*. (IM 40) Lanham, MD: Asphalt Pavement Alliance.

Nunn, M. E., Brown, A., Weston, D., & Nicholls, J. C. (1997). *Design of Long-Life Flexible Pavements for Heavy Traffic*. *TRL REPORT 250*.

Prowell, B., Brown, E. R., Anderson, R. M., Daniel, J. S., Von Quintus, H., Shen, S., ... & Maghsoodloo, S. (2010). NCHRP Report 646: Validating the Fatigue Endurance Limit for Hot Mix Asphalt. *Transportation Research Board of the National Academies, Washington, DC*.

Roberts, F. L., Mohammad, L. N., & Wang, L. B. (2002). History of hot mix asphalt mixture design in the United States. *Journal of Materials in Civil Engineering*, *14*(4), 279-293.

Romanello, M. (2007). *Load Response Analysis of the WAY-30 Test Pavements: US Route 30, Wayne County, Ohio.* (Electronic Thesis or Dissertation). Retrieved from https://etd.ohiolink.edu/.

Romanoschi, S. A., Gisi, A. J., & Dumitru, C. (2006). The dynamic response of Kansas perpetual pavements under vehicle loading. *Paper presented at the Proceedings for the International Conference on Perpetual Pavements, Columbus, OH.*

Sargand, S., & Edwards, W. (2010). David Lankard, consultant. *Forensic Investigation of AC and PCC Pavement with Extended Service Life.* (No. FHWA/OH-2010/004A). Ohio Department of Transportation.

Sargand, S., Figueroa, J. L., Edwards, W., & Al-Rawashdeh, A. S. (2009). *Performance assessment of warm mix asphalt (WMA) pavements* (No. FHWA/OH-2009/08). Ohio Research Institute for Transportation and the Environment.

Sargand, S., Khoury, I., Gray, J., & Al-Jhayyish, A. (2014). *Incorporating Chemical Stabilization of the Subgrade in Pavement Design and Construction Practices* (No. FHWA/OH-2014/12).

Scheer, M. J. (2013). *Impact of Pavement Thickness on Load Responses of Perpetual Pavement.* (Unpublished MS thesis), Ohio University, Athens, OH.

Tarefder, R. A., & Bateman, D. (2009). Determining the optimal perpetual pavement structure. Ohio Research Institute for Transportation and the Environment (ORITE). *Paper presented at the Proceedings for the International Conference on Perpetual Pavement. Columbus, OH*.

Tarefder, R. & Bateman, D. (2012). ”Design of Optimal Perpetual Pavement Structure.” *Journal of Transportation Engineering., 138(2) 157-175*

Thompson, M. R., & Carpenter, S. H. (2006). *Considering hot-mix-asphalt fatigue endurance limit in full-depth mechanistic-empirical pavement design*. *Urbana*, *51*, 61801-2350.

Timm, D. H., & Newcomb, D. E. (2006). Perpetual pavement design for flexible pavements in the US. *International Journal of Pavement Engineering*, *7*(2), 111-119.

Timm, D. H., Robbins, M. M., & Kluttz, R. Q. (2011). Full-Scale Structural Characterization of a Highly Polymer-Modified Asphalt Pavement. In *Transportation Research Board 90th Annual Meeting* (No. 11-1069).

Timm, D. H., Robbins, M. M., Willis, J. R., Tran, N., & Taylor, A. J. (2013). *Field and Laboratory Study of High-Polymer Mixtures at the NCAT Test Track Final Report* (No. 13-03).

Transportation Officials. (1993). *AASHTO Guide for Design of Pavement Structures, 1993* (Vol. 1). AASHTO.

Von Quintus, H. L., (2001). Hot-Mix Asphalt Layer Thickness Design for Longer-Life Bituminous Pavement. *Transportation Research Circular*, *503*, 66-78.

Willis, J. R., Taylor, A., Tran, N. H., Kluttz, B., Timm, D. H. (2012). Laboratory Evaluation of High Polymer Plant-Produced Mixtures. *Proceedings from Transportation Research Board Annual Meeting, 2012, Washington, D.C*

Willis, R., Timm, D., West, R., Powell, B., Robbins, M., Taylor, A., ... & Bianchini, A. (2009). Phase III NCAT test track findings. *National Center for Asphalt Technology. Auburn University, Alabama*.

Witczak, M., Mamlouk, M., Souliman, M., & Zeiada, W. (2013). *Laboratory Validation of an Endurance Limit for Asphalt Pavements* (No. Project 9-44A).

Yildirim, Y. (2007). Polymer modified asphalt binders. *Construction and Building Materials*, *21*(1), 66-72.

APPENDIX A: PEAK STRAINS

Table A.1 Peak Strains for APLF Test Sections at 70° F (21.1° C) at 6000 lb (27 kN)

Test Run	Long. AC Base		Trans. AC Base		Long. Intermediate	Trans. Intermediate
	KMB-001	KMB-003	KMB-02	KMB-04	KMB-005	KMB-06
Lane A						
A01A-0001	38	35	8	8	-15	-15
A01A-0002	43	38	9	8	-16	-16
A01A-0003	38	36	8	8	-15	-16
A02-0001	33	35	7	8	-16	-12
A02-0002	35	33	7	7	-16	-12
A02-0003	36	33	7	7	-16	-12
A03-0001	32	32	6	6	-18	-11
A03-0002	34	32	6	6	-17	-11
A03-0003	34	31	8	8	-17	-15
Lane B						
B01-0001	34	36	7	9	-17	-
B01-0002	34	36	7	9	-18	-
B01-0003	34	35	7	9	-18	-
B02-0001	28	30	6	7	-17	-
B02-0002	28	29	5	7	-17	-
B02-0003	29	30	5	7	-17	-
B03-0001	30	32	7	10	-15	-
B03-0002	29	30	6	8	-15	-
B03-0003	29	29	5	7	-17	-
Lane C						
C01-0001	23	23	11	11	-24	-
C01-0002	24	24	11	11	-23	-
C01-0003	24	24	11	11	-23	-
C02-0001	20	22	10	12	-19	-
C02-0002	22	23	10	11	-20	-
C02-0003	22	22	10	11	-21	-
C03-0001	17	19	8	10	-13	-
C03-0002	17	18	8	9	-16	-

C03-0003	18	18	8	9	-18	-
Lane D						
D01-0001	22	24	10	9	-20	-
D01-0002	23	23	9	9	-20	-
D01-0003	23	23	9	9	-20	-
D02A-0001	29	42	28	21	-7	-
D02A-0002	30	43	29	22	-7	-
D02A-0003	30	43	29	22	-7	-
D03-0001	23	23	8	9	-21	-
D03-0002	23	23	8	8	-21	-
D03-0003	23	24	8	8	-21	-

Table A.2 Peak Strains for APLF Test Sections at 70° F (21.1° C) at 9000 lb (40 kN)

Test Run	Long. AC Base		Trans. AC Base		Long. Intermediate	Trans. Intermediate
	KMB-001	KMB-003	KMB-02	KMB-04	KMB-005	KMB-06
Lane A						
A01A-0013	60	54	12	11	-24	-22
A01A-0014	59	53	12	11	-24	-23
A01A-0015	61	53	12	11	-24	-23
A02-0013	57	51	11	10	-24	-19
A02-0014	58	52	11	11	-24	-20
A02-0015	58	51	11	11	-25	-20
A01-0013	55	49	9	9	-26	-18
A01-0014	56	49	9	9	-25	-18
A01-0015	55	49	10	9	-26	-18
Lane B						
B01-0013	52	54	11	13	-26	-
B01-0014	52	53	11	13	-26	-
B01-0015	52	53	11	13	-25	-
B02-0013	46	47	9	11	-26	-
B02-0014	46	46	9	11	-26	-
B02-0015	47	47	9	11	-26	-
B03-0013	46	47	8	12	-25	-
B03-0014	46	46	9	11	-26	-
B03-0015	46	46	9	11	-26	-
Lane C						
C01-0013	37	36	18	17	-35	-
C01-0014	38	37	17	18	-34	-
C01-0015	39	36	18	17	-35	-
C02-0013	37	36	16	18	-30	-
C02-0014	37	35	16	18	-31	-
C02-0015	37	35	16	17	-31	-
C03-0013	31	31	13	14	-26	-
C03-0014	31	31	12	14	-27	-
C03-0015	32	31	13	14	-29	-

Lane D						
D01-0013	38	37	16	15	-31	-
D01-0014	38	37	16	15	-30	-
D01-0015	38	38	18	15	-30	-
D02A-0013	39	55	35	25	-18	-
D02A-0014	39	55	34	25	-17	-
D02A-0015	39	55	35	24	-18	-
D03-0013	37	36	13	13	-33	-
D03-0014	38	37	13	14	-33	-
D03-0015	37	36	13	13	-34	-

Table A.3 Peak Strains for APLF Test Sections at 70° F (21.1° C) at 12,000 lb (53 kN)

Test Run	Long. AC Base		Trans. AC Base		Long. Intermediate	Trans. Intermediate
	KMB-001	KMB-003	KMB-02	KMB-04	KMB-005	KMB-06
Lane A						
A01A-0025	78	69	16	15	-31	-29
A01A-0026	78	68	16	15	-31	-30
A01A-0027	79	67	16	15	-30	-30
A02-0025	75	65	14	13	-31	-25
A02-0026	75	64	14	13	-32	-26
A02-0027	75	65	14	13	-32	-26
A01-0025	72	62	12	10	-34	-24
A01-0026	72	62	12	11	-34	-24
A01-0027	72	62	12	11	-34	-24
Lane B						
B01-0025	68	69	15	17	-31	-
B01-0026	68	68	15	17	-31	-
B01-0027	68	68	16	17	-31	-
B02-0025	59	60	12	14	-33	-
B02-0026	60	60	12	14	-34	-
B02-0027	60	60	13	14	-33	-
B03-0025	58	59	11	15	-32	-
B03-0026	58	58	12	15	-33	-
B03-0027	59	59	12	14	-33	-
Lane C						
C01-0025	51	48	23	24	-43	-
C01-0026	50	48	23	24	-43	-
C01-0027	51	48	24	24	-43	-
C02-0025	48	46	21	23	-39	-
C02-0026	49	46	21	24	-39	-
C02-0027	49	46	20	23	-40	-
C03-0025	42	41	17	19	-34	-
C03-0026	42	41	17	20	-35	-
C03-0027	42	41	17	19	-35	-

Lane D						
D01-0025	51	50	22	21	-40	-
D01-0026	51	50	23	21	-40	-
D01-0027	51	52	25	22	-39	-
D02A-0026	51	64	41	26	-26	-
D02A-0027	51	67	40	28	-26	-
D02A-0028	51	66	40	27	-27	-
D03-0025	49	47	18	17	-43	-
D03-0026	49	47	18	17	-43	-
D03-0027	49	47	18	17	-43	-

Table A.4 Peak Strains for APLF Test Sections at 100° F (37.8° C) at 6000 lb (27 kN)

Test Run	Long. AC Base		Trans. AC Base		Long. Intermediate	Trans. Intermediate
	KMB-001	KMB-003	KMB-02	KMB-04	KMB-005	KMB-06
Lane A						
A04A-0002	57	56	-17	-25	-58	-16
A04A-0003	59	58	-17	-25	-57	-16
A04A-0004	59	57	-17	-27	-59	-16
A05-0001	64	64	-12	-21	-60	-12
A05-0002	65	61	-14	-22	-58	-16
A05-0003	63	61	-14	-22	-58	-17
A06-0001	64	66	-12	-21	-61	-14
A06-0002	66	63	-12	-21	-61	-17
A06-0003	64	63	-14	-21	-62	-18
Lane B						
B07A-0003	32	38	-16	-13	-63	-
B07A-0004	35	38	-15	-13	-63	-
B07A-0005	36	38	-15	-12	-60	-
B08-0001	41	42	-12	-8	-65	-
B08-0002	41	42	-12	-9	-68	-
B08-0003	41	44	-12	-8	-68	-
B09-0001	43	41	-12	-14	-67	-
B09-0002	44	46	-11	10	-67	-
B09-0003	44	46	-11	11	-66	-
Lane C						
C10-0001	32	32	-9	-7	-47	-
C10-0002	32	33	-6	-6	-51	-
C10-0003	31	33	-5	-6	-54	-
C11-0001	41	44	5	7	-50	-
C11-0002	37	40	-3	5	-63	-
C11-0003	36	41	-4	5	-71	-
C12-0001	26	25	-9	-8	-24	-

C12-0002	29	34	3	7	-34	-
C12-0003	29	33	3	7	-44	-
Lane D						
D13-0001	29	34	-2	-9	-61	-
D13-0002	28	34	-3	-9	-59	-
D13-0003	27	34	-3	-9	-58	-
D14A-0004	25	28	-2	-7	-51	-
D14A-0005	25	28	-2	-6	-52	-
D14A-0006	26	28	-2	-7	-51	-
D14B-0001	21	23	-1	-6	-46	-
D14B-0002	22	23	-2	-7	-47	-
D14B-0003	22	24	-2	-7	-48	-

Table A.5 Peak Strains for APLF Test Sections at 100° F (37.8° C) at 9000 lb (40 kN)

Test Run	Long. AC Base		Trans. AC Base		Long. Intermediate	Trans. Intermediate
	KMB-001	KMB-003	KMB-02	KMB-04	KMB-005	KMB-06
Lane A						
A04A-0014	89	85	-37	-51	-91	-28
A04A-0015	90	86	-31	-43	-91	-29
A04A-0016	90	85	-30	-43	-94	-29
A05-0013	91	87	-31	-41	-96	-28
A05-0014	91	86	-25	-36	-96	-29
A05-0015	93	85	-24	-35	-94	-28
A06-0013	92	88	-32	-45	-101	55
A06-0014	92	91	-26	-37	-100	-32
A06-0015	92	90	-24	-35	-98	-33
Lane B						
B07A-0015	59	59	-28	-24	-90	-
B07A-0016	60	59	-23	-18	-90	-
B07A-0017	61	59	-23	-17	-90	-
B08-0013	61	61	-25	-19	-99	-
B08-0014	63	65	-21	-13	-100	-
B08-0015	63	66	-20	-12	-97	-
B09-0013	61	55	-35	-35	-107	-
B09-0014	63	73	-23	17	-102	-
B09-0015	65	73	-21	17	-102	-
Lane C						
C10-0013	48	48	-8	-11	-79	-
C10-0014	49	50	-7	-9	-81	-
C10-0015	49	50	-7	-8	-82	-
C11-0013	52	56	-3	8	-94	-
C11-0014	52	56	-5	-8	-99	-
C11-0015	52	56	-4	8	-102	-
C12-0013	45	50	-3	7	-75	-

C12-0014	44	48	-4	-6	-83	-
C12-0015	44	48	-3	6	-89	-
Lane D						
D13-0013	44	51	-8	-17	-91	-
D13-0014	44	55	6	-14	-89	-
D13-0015	43	56	16	-14	-84	-
D14A-0016	42	45	-6	-13	-82	-
D14A-0017	41	45	-4	-12	-82	-
D14A-0018	42	45	-4	-11	-83	-
D14B-0013	37	38	-6	-13	-75	-
D14B-0014	37	38	-4	-12	-77	-
D14B-0015	38	39	-4	-11	-76	-

Table A.6 Peak Strains for APLF Test Sections at 100° F (37.8° C) at 12,000 lb (53 kN)

Test Run	Long. AC Base		Trans. AC Base		Long. Intermediate	Trans. Intermediate
	KMB-001	KMB-003	KMB-02	KMB-04	KMB-005	KMB-06
Lane A						
A04A-0026	112	107	-47	-64	-119	-40
A04A-0027	112	106	-42	-59	-121	-41
A04A-0028	113	106	-38	-59	-118	-40
A05-0025	107	100	-40	-55	-121	-38
A05-0026	107	102	-33	-48	-115	-41
A05-0027	107	103	-30	-46	-114	-42
A06-0025	106	102	-44	-56	-128	-42
A06-0026	105	104	-35	-49	-126	56
A06-0027	106	103	-33	-48	-123	-43
Lane B						
B07A-0027	80	73	-36	-28	-112	-
B07A-0028	80	74	-31	-22	-116	-
B07A-0029	81	75	-29	-22	-108	-
B08-0025	78	78	-31	-23	-126	-
B08-0026	79	77	-27	-18	-121	-
B08-0027	81	81	-26	-14	-120	-
B09-0025	77	82	-34	-26	-119	-
B09-0026	78	83	-29	-20	-122	-
B09-0027	79	83	-28	-19	-120	-
Lane C						
C10-0025	62	61	-11	-14	-97	-
C10-0026	63	63	-10	-12	-95	-
C10-0027	64	64	-9	-11	-97	-
C11-0025	64	67	-6	-10	-116	-
C11-0026	63	67	-7	-10	-123	-
C11-0027	63	66	-6	9	-126	-

C12-0025	55	57	-8	-13	-102	-
C12-0026	54	58	-5	-8	-109	-
C12-0027	54	59	-6	-8	-115	-
			Lane D			
D13-0025	58	68	-11	-21	-113	-
D13-0026	58	70	14	-19	-111	-
D13-0027	58	73	17	-19	-103	-
D14A-0028	54	57	-9	-19	-101	-
D14A-0029	54	58	-6	-16	-96	-
D14A-0030	54	59	-6	-15	-94	-
D14B-0025	49	50	-9	-18	-94	-
D14B-0026	48	50	-6	-16	-93	-
D14B-0027	49	51	-6	-16	-92	-

Note: Transverse gauges in the intermediate layers for Lane B, Lane C, and Land D were damaged during construction

APPENDIX B: WHEEL WANDERING TABLES

Table B.1 Maximum Longitudinal AC Base Layer Strain at "0" Offset

Lane	AC Thickness (in)	AC Thickness (cm)	Load (lbs (kN)) 6000 (27) *Avg*	6000 (27) *Max*	9000 (40) *Avg*	9000 (40) *Max*	12000 (53) *Avg*	12000 (53) *Max*
70° F (21.1° C)								
A	**8**	**20**	35	43	54	61	70	79
B	**9**	**23**	31	36	48	54	62	69
C	**10**	**25**	21	24	35	39	46	51
D	**11**	**28**	27	43	40	55	52	67
100° F (37.8° C)								
A	**8**	**20**	62	66	89	93	106	113
B	**9**	**23**	41	46	63	73	79	83
C	**10**	**25**	34	44	50	56	61	67
D	**11**	**28**	27	34	43	56	56	73

Table B.2 Maximum Longitudinal AC Base Layer Strain at "-2" Offset

Lane	AC Thickness (in)	AC Thickness (cm)	Load (lbs (kN)) 6000 (27) *Avg*	6000 (27) *Max*	9000 (40) *Avg*	9000 (40) *Max*	12000 (53) *Avg*	12000 (53) *Max*
70° F (21.1° C)								
A	**8**	**20**	36	38	55	60	71	79
B	**9**	**23**	32	38	49	55	63	71
C	**10**	**25**	22	25	35	39	46	51
D	**11**	**28**	28	43	41	57	54	68
100° F (37.8° C)								
A	**8**	**20**	62	66	89	91	107	112
B	**9**	**23**	42	49	64	72	81	84
C	**10**	**25**	33	38	49	53	61	66
D	**11**	**28**	28	38	44	58	58	75

Table B.3 Maximum Longitudinal AC Base Layer Strain at "-6" Offset

Lane	AC Thickness (in)	AC Thickness (cm)	Load (lbs (kN)) 6000 (27) Avg	6000 (27) Max	9000 (40) Avg	9000 (40) Max	12000 (53) Avg	12000 (53) Max
70° F (21.1° C)								
A	**8**	**20**	38	41	58	63	73	82
B	**9**	**23**	35	40	52	57	65	74
C	**10**	**25**	22	25	35	39	46	50
D	**11**	**28**	28	43	38	57	53	69
100° F (37.8° C)								
A	**8**	**20**	68	71	95	99	111	120
B	**9**	**23**	47	55	68	76	82	87
C	**10**	**25**	33	37	48	52	60	65
D	**11**	**28**	29	39	45	59	58	77

Table B.4 Maximum Longitudinal AC Base Layer Strain at "-12" Offset

Lane	AC Thickness (in)	AC Thickness (cm)	Load (lbs (kN)) 6000 (27) Avg	6000 (27) Max	9000 (40) Avg	9000 (40) Max	12000 (53) Avg	12000 (53) Max
70° F (21.1° C)								
A	**8**	**20**	28	33	44	51	57	66
B	**9**	**23**	30	33	44	47	56	60
C	**10**	**25**	18	20	29	32	39	42
D	**11**	**28**	24	41	36	52	47	64
100° F (37.8° C)								
A	**8**	**20**	49	53	71	78	86	99
B	**9**	**23**	41	44	57	60	69	76
C	**10**	**25**	26	30	39	43	49	54
D	**11**	**28**	24	30	37	46	49	62

APPENDIX C: WHEEL WANDERING FIGURES

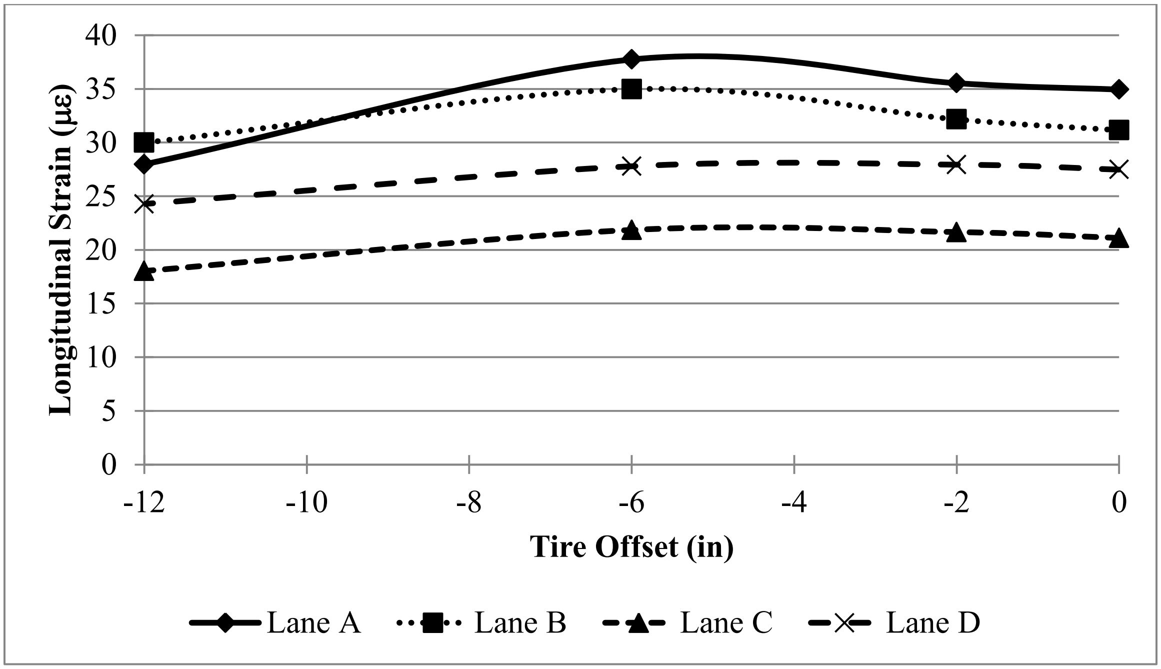

Figure C.1 Average Longitudinal Strain Produced by Varying Tire Offset 70° F (21.1° C) at 6000 lb (27 kN)

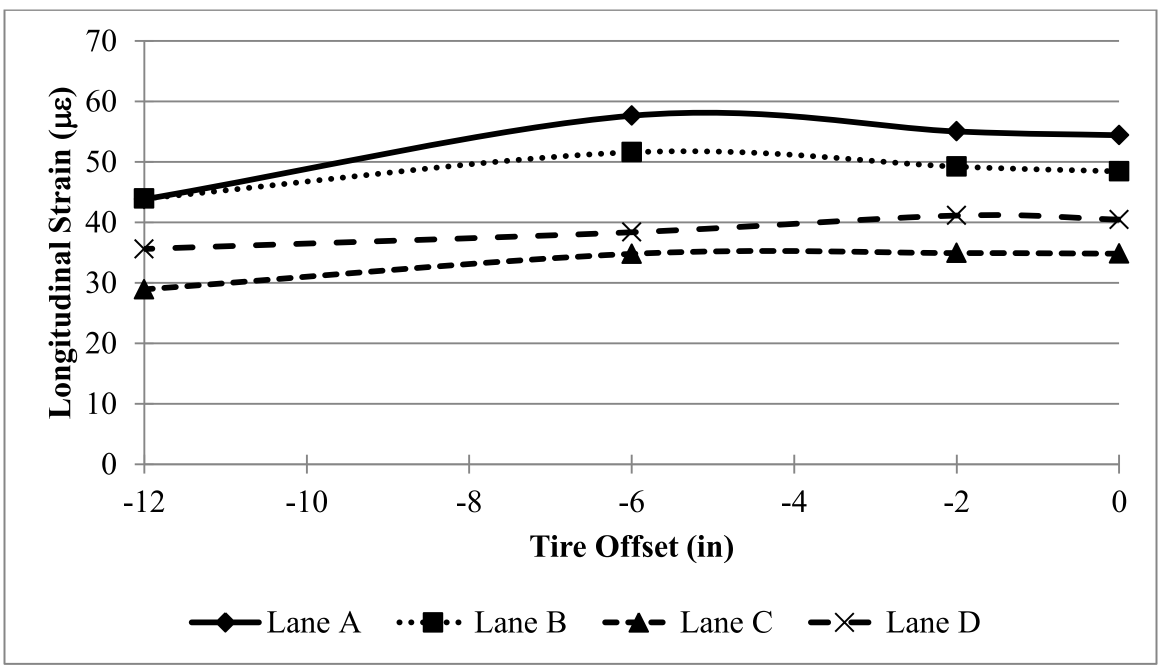

Figure C.2 Average Longitudinal Strain Produced by Varying Tire Offset 70° F (21.1° C) at 9000 lb (40 kN)

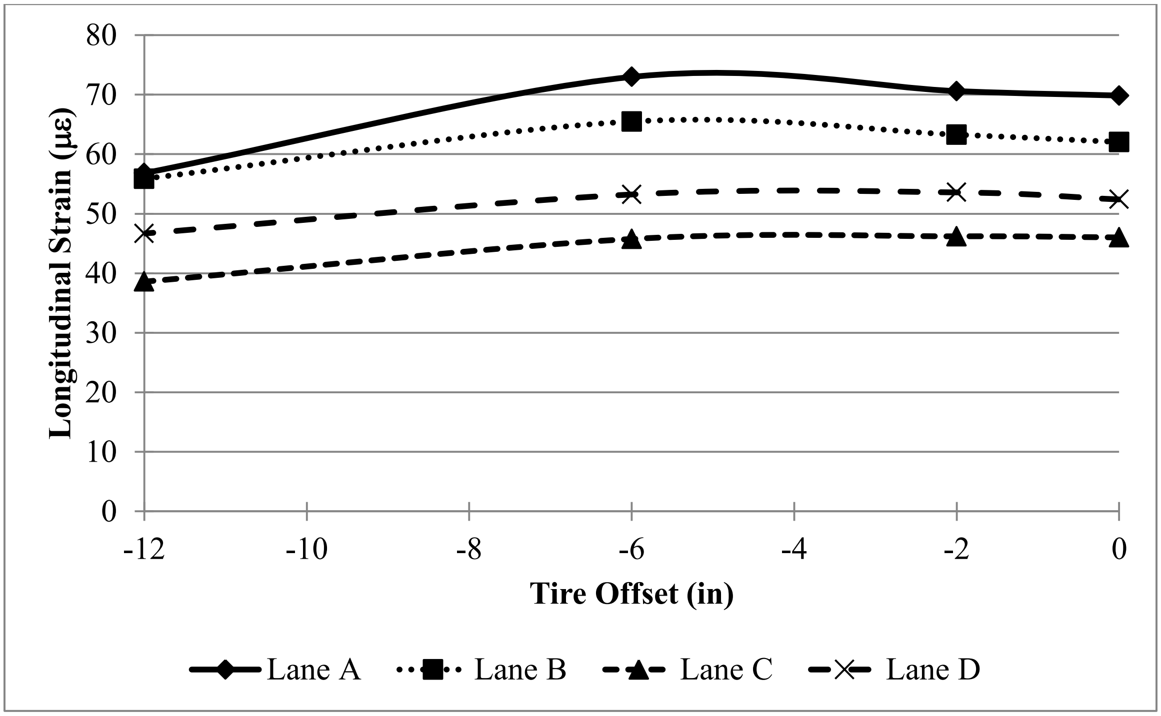

Figure C.3 Average Longitudinal Strain Produced by Varying Tire Offset 70° F (21.1° C) at 12,000 lb (53 kN)

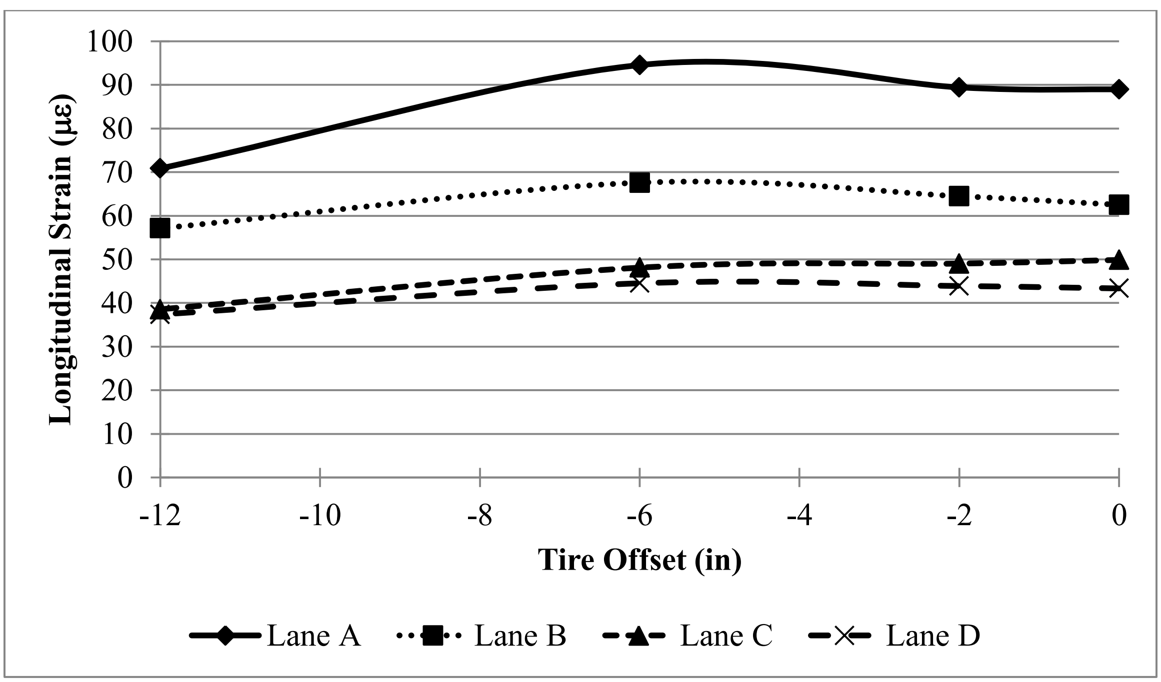

Figure C.4 Average Longitudinal Strain Produced by Varying Tire Offset 100° F (37.8° C) at 9000 lb (40 kN)

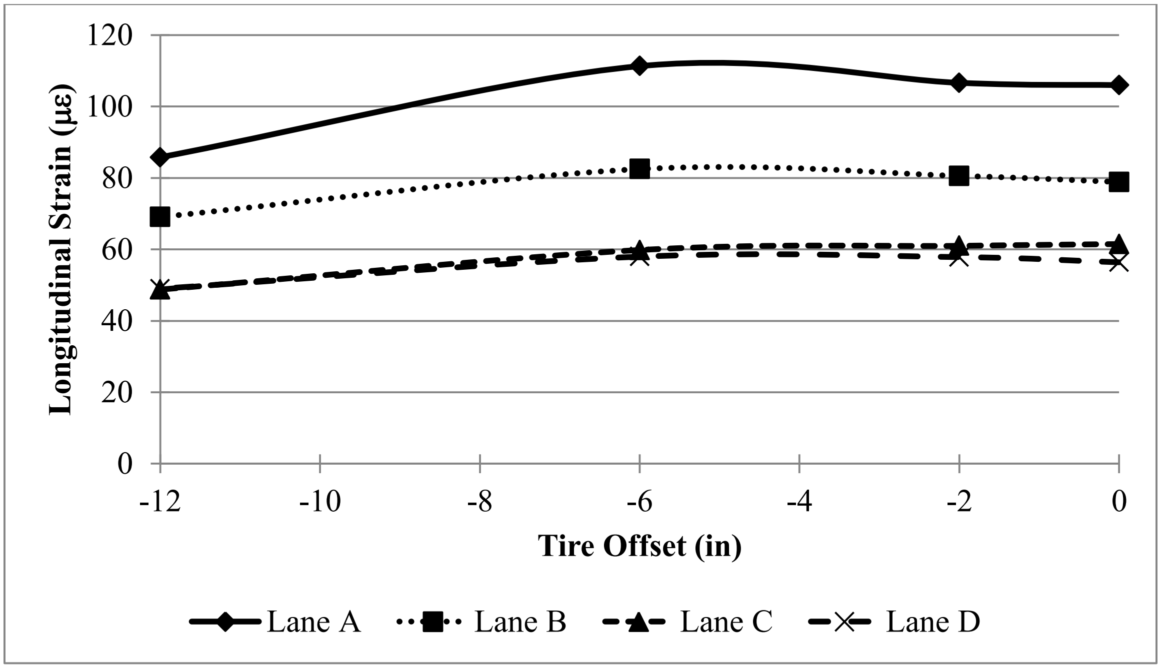

Figure C.5 Average Longitudinal Strain Produced by Varying Tire Offset 100° F (37.8° C) at 12000 lb (53 kN)

APPENDIX D: GAUGE LIST AND LOADING LOG

Table D.1 APLF Strain Gauge List

Gauge #	LANE	Location off Pavement	Layer	Trans or Long
EKZ130747	A	1	Base	Long.
EKZ130748	A	2	Base	Trans.
EKZ130749	A	3	Base	Long.
EKZ130750	A	4	Base	Trans.
EKZ130751	A	2	Intermediate	Trans.
EKZ130759	A	3	Intermediate	Long.
EKZ130741	B	1	Base	Long.
EKZ130742	B	2	Base	Trans.
EKZ130743	B	3	Base	Long.
EKZ130744	B	4	Base	Trans.
EKZ130745	B	2	Intermediate	Trans.
EKZ130746	B	3	Intermediate	Long.
EKZ130734	C	1	Base	Long.
EKZ130735	C	2	Base	Trans.
EKZ130736	C	3	Base	Long.
EKZ130737	C	4	Base	Trans.
EKZ130739	C	2	Intermediate	Trans.
EKZ130740	C	3	Intermediate	Long.
EKZ130728	D	1	Base	Long.
EKZ130729	D	2	Base	Trans.
EKZ130730	D	3	Base	Long.
EKZ130731	D	4	Base	Trans.
EKZ130732	D	2	Intermediate	Trans.
EKZ130733	D	3	Intermediate	Long.

Table D.2 APLF Loading Run Log

Run Log	Passes	Lane	Date	Comments
HIMA D01	100	D	May 02, 2014	
HIMA D02	3000	D	May 06, 2014	Missed Passes after 20
HIMA D02A	" "	" "	May 06, 2014	25 bad file, +1 file numbers
HIMA D03	10000	D	May 13, 2014	LVDT 1- wrong channel
HIMA C01	100	C	May 13, 2014	
HIMA C02	3000	C	May 15, 2014	
HIMA C03	10000	C	May 28, 2014	
HIMA B01	100	B	May 28, 2014	
HIMA B02	3000	B	Jun. 02, 2014	
HIMA B03	10000	B	Jun. 06, 2014	
HIMA A01A	100	A	Jun. 06, 2014	
HIMA A02	3000	A	Jun. 10, 2014	
HIMA A03	10000	A	Jun. 18, 2014	
HIMA A04	100	A	Jul. 07, 2014	Stopped after 30, wheel malfunction
HIMA A04A	" "	" "	Jul. 08, 2014	1 bad file, +1 file numbers
HIMA A05	3000	A	Aug. 04, 2014	
HIMA A06	10000	A	Aug. 06, 2014	
HIMA B07	100	B	Aug. 07, 2014	Stopped after 24, LVDT 1 loose
HIMA B07A	" "	" "	Aug. 07, 2014	1 and 2 bad Files, +2 file numbers
HIMA B08	3000	B	Aug. 12, 2014	
HIMA B09	10000	B	Aug. 20, 2014	
HIMA C10	100	C	Aug. 20, 2014	
HIMA C11	3000	C	Aug. 21, 2014	
HIMA C12	10000	C	Sept. 03, 2014	
HIMA D13	100	D	Sept. 03, 2014	
HIMA D14	3000	D	Sept. 08, 2014	Corrected LVDT
HIMA D14A	" "	" "	Sept. 08, 2014	First 3 files bad, +3 file numbers
HIMA D14B	10000	D	Sept. 24, 2014	